2011

Initial Ablation of the Laurentide Ice Sheet Based on Gulf of Mexico Sediments

Elizabeth A. Brown
University of South Florida, eabrown@mail.usf.edu

Initial Ablation of the Laurentide Ice Sheet

Based on Gulf of Mexico Sediments

by

Elizabeth A. Brown

A thesis submitted in partial fulfillment
of the requirements for the degree of
Master of Science
College of Marine Science
University of South Florida

Major Professor: Benjamin P. Flower, Ph.D.
David W. Hastings, Ph.D.
Sang-Ik Shin, Ph.D.

Date of Approval:
July 12, 2011

Keywords: Last Glacial Maximum, Orca Basin, deglaciation, geochemical proxies, *Globigerinoides ruber*

DEDICATION

I dedicate this thesis with deepest thanks to my family, friends, and everyone who has encouraged me and backed me up these last two years of graduate school. Most especially, to my parents Joshua K. Brown and Joyce Leacy Brown for your inexhaustible positive reinforcement and your intellectual, emotional, and occasionally financial support, and to my marvelous Matthew, the most amazingly awesome brother on the face of this earth ("This was a triumph…").

Special thanks to Jenni, Esa-Matti & Greg for being fabulous and hilarious, providing me with intermittent means of escape on the weekends – oh, those many weekends – keeping me on track on the weekdays, making fun of me when I needed it, and making me laugh. To Mari and Gaby, Juan Carlos and Claudia, Nat, Ana and the girls for love, communal panic, and lots of giant group-style suppers. Just what every graduate student needs. Thanks as well to Dwight, Tim, Rev. Jamie, Rev. Stephen, and the entire choir of St. Peter's Episcopal Cathedral for being both my extracurricular break and my spiritual haven from academia.

ACKNOWLEDGMENTS

I would like to express my appreciation and my gratitude to Dr. Benjamin P. Flower for the opportunities and guidance he has provided me at the College of Marine Science, and his enduring patience along the way. I would also like to thank Drs. David Hastings and Sang-Ik Shin for lending me their expertise as I puzzled through this research project.

I owe huge thanks to Ethan Goddard for every part of this study's labwork he's helped me with, however complicated or however mundane; without him, the Paleoceanography lab wouldn't run. Carlie Williams has also provided me with lots of guidance, especially in chemical preparation, sample cleaning techniques, and raw data processing, and the upper half of core MD02-2550 discussed throughout this thesis is her work. Kelly Quinn has given me many hours of her time, running the ICP-MS for my Mg/Ca analyses. I would like to thank them, and the entire Paleoceanography & Biogeochemistry lab for keeping me moving forward.

Much of the discussion section in this paper is the product of conversations with Don Chambers, Mindy Robinson, Jennifer Bonin, Esa-Matti Tastula and Yingli Zhu, providing me with insight into meteorological systems, the ITCZ, and atmosphere-ocean dynamics. Thanks to Yingli for help with map-making programs as well.

This research was funded in part, by the Peter R. Betzer Fellowship, and by NSF Grant OCE-0903017 to Dr. Flower.

TABLE OF CONTENTS

LIST OF TABLES

LIST OF FIGURES

ABSTRACT

The objective of this project is to reconstruct a picture of initial Laurentide Ice Sheet retreat at the end of the Last Glacial Maximum (LGM) using geochemical proxies in Gulf of Mexico sediments, and place the reconstruction into global perspective. The project asks two questions. (1) Can a time frame be established for initial retreat of the Laurentide Ice Sheet? (2) If so, how does the timing compare to that of other large ice sheets and mountain glaciers in both hemispheres?

Sediment core MD02-2550 from the anoxic Orca Basin offers excellent preservation and a high sediment accumulation rate. Twelve accelerator mass spectrometry ^{14}C dates provide very good age control from 18.36 – 23.88 ka, the transitional period from glacial to deglacial conditions. Paired Mg/Ca and $\delta^{18}O$ from the planktonic foraminifera *Globigerinoides ruber* (pink variety) were combined with a matching record from the upper half of the same core from a previous study (Williams et al., 2010), expanding the record to 10.73 – 23.86 ka.

Sea surface temperature (SST) derived from Mg/Ca exhibits a mean value of 23.0 ± 0.8°C through the LGM (18.4-23.9 ka), ~3.9°C below the modern summer mean. At 18.4 ka, mean values drop in an anomalous cold snap, exhibiting a mean of 21.7°C that lasted until 17.8 ka. At 17.8 ka, SST begins a recovery warming toward present day

conditions. This warming occurs markedly early relative to the onset of the Bølling-Allerød warm period, known best from Greenland ice core records.

The $\delta^{18}O$ of seawater exhibits no sustained shift toward more depleted values that would be consistent with a single major surge of initial meltwater. Instead, $\delta^{18}O_{sw}$ appears to have been over 1.5‰ below the modern mean throughout the LGM, persisting through the early deglacial period, and not shifting toward more positive values until well into the Younger Dryas. The corresponding salinity estimates were likewise ~2 psu lower than modern surface waters. Several negative excursions (~1‰) during the LGM and deglaciation coincide with millennial-scale retreats of individual lobes along the southern margin of the Laurentide Ice Sheet. These retreats and re-advances have previously been suggested to mirror small short-term excursions in Greenland ice core $\delta^{18}O$, that reflects air temperature changes.

The consistently depleted $\delta^{18}O_{sw\text{-}ivc}$ values and corresponding salinity estimates through the LGM require a mechanism to create a steady-state lower salinity environment in the northern Gulf of Mexico during the LGM, which would persist as SST changed.

INTRODUCTION

The last glacial maximum (hereafter LGM), is conventionally defined as the period spanning ~26.5 to 19 thousand years ago, when continental ice sheets in both the northern and southern hemispheres were collectively at their greatest volume and latitudinal extent (Mix et al., 2001; Dyke et al., 2002; Clark et al., 2009; Denton et al., 2010). In the northern hemisphere, the large ice sheets included the Laurentide, Cordilleran, Greenland, Fennoscandian, Barents and Kara Ice Sheets. Global sea level was an estimated 120 – 134 meters lower than present (Denton and Hughes, 1981; Fairbanks, 1989; Clark and Mix, 2002). Most of this impact came from northern hemisphere ice sheets, forming up to 120 meters sea-level equivalent ice volume.

In North America, the Laurentide Ice Sheet (hereafter LIS) reached a southern extent of nearly 40° latitude (Anderson et al., 2002; Clark and Mix, 2002). The LIS comprised seven smaller regional ice sheets or lobes, some of which reached individual maxima as early as 33 ka. These seven sections (the Mackenzie River Lobe, the Northeastern Margin, the Des Moines Lobe, Lake Michigan Lobe, Ohio-Erie-Ontario Lobe, Maritime Provinces region and New England region) began to merge between 33 and 29 ka. Indeed, radiocarbon data from Dyke et al. (2002) suggest that the LIS attained a latitudinal maximum before the global LGM, as early as 29 – 27 ka.

The LIS was also by far the largest of the ice sheets in the northern hemisphere during the LGM; collectively, the components of the LIS attained maximum ice volume

between 15.9 – 37 x 10^6 km^3, or ~40 – 90 m sea-level equivalent (Kennett & Shackleton 1975; Liccardi et al., 1998; Mix et al., 2001; Dyke et al., 2002), and retained a steady-state size throughout the LGM. The Fennoscandian was the second-largest, with an estimated volume of only 6.9 x 10^6 km^3 accounting for 13 – 18 m sea-level equivalent (Lambeck 1995; Siegert et al., 1999; Clark and Mix, 2002). The Antarctic ice sheet in the southern hemisphere was volumetrically larger, but during deglaciation, the size of the Antarctic ice sheet changed little by comparison to those in the northern hemisphere, ranging from 14 m sea-level equivalent as a low end estimate, to 20 – 30 m as a high end estimate (Denton and Hughes, 1981; Nakada and Lambeck, 1988; Anderson et al., 2002; Denton and Hughes, 2002; Clark and Mix, 2002; Denton et al., 2010).

The LIS is therefore of monumental importance when considering the termination of the LGM, the melting of the great ice sheets, and ultimately, their contributions to changes in sea level and climate. Besides being an enormous topographical feature with the potential to change size on a geologically rapid time scale, the LIS probably influenced climate by displacing the jet streams and creating anti-cyclonic systems at the ice sheet surface (Manabe and Broccoli, 1985b; Pollard and Thompson, 1997), acting as a reservoir for vast amounts of fresh water capable of altering thermohaline circulation and ocean heat budget in both hemispheres (Crowley 1992; Stocker 1998; Chiang et al., 2003; Knutti et al., 2004), and by affecting albedo, local radiation budget, and local air temperature (Clark et al., 1999).

Last Glacial Termination

Denton et al. (2010) noted that the recession of the continental ice sheets covering much of North America and northern Europe to the present state (that is, covering only parts of Greenland and most of Antarctica), represents one of the fastest natural climate changes in recent geologic history: at 20 ka, continental ice was at a maximum. Between 19 – 17 ka, as inferred from $\delta^{18}O$ and δD air temperature proxies in Antarctic ice cores (e.g. Petit et al., 1999; Blunier and Brook, 2001, Monnin et al., 2001), global air temperature began to rise, and the ice sheets began a retreat which would eventually lead to their present day conditions. By 11 ka, Antarctic ice volume and air temperature had reached modern interglacial conditions. By 7 ka, the Fennoscandian, Cordilleran, Kara and Barents ice sheets were gone, and only a small fragment of the LIS remained, on Baffin Island (Dyke and Prest, 1987; Anderson et al., 2002; Dyke et al., 2002; Denton et al., 2010).

One prominent feature of the last glacial termination records is that initial warming of the northern and southern hemispheres appears to have been asynchronous. $\delta^{18}O$ and δD from Antarctic EPICA Dome C, Byrd Dome, Vostok and Komsomolska ice cores exhibit a sustained trend toward more positive values beginning between 17 and 19 ka (e.g. Steig et al., 1998; Blunier and Brook, 2001; Jouzel et al., 2001; Monnin et al., 2001). Air temperatures decreased for almost 2 thousand years in the Antarctic Cold Reversal episode between ~12 and 14 ka, then began to rise again shortly before the onset of the Younger Dryas ~12.5 ka.

Conversely, in the northern hemisphere, $\delta^{18}O$ and δD measured in Greenland Ice Sheet Project 2 (GISP2) core records from Greenland indicate a persistence of stadial

conditions throughout the Oldest Dryas until 14.67 ka. At this point, Greenland records exhibit a sharp increase in air temperature, marking the onset of the Bølling-Allerød (Grootes and Stuiver, 1997; Steig et al., 1998; Stuiver and Grootes, 2000). This coincides roughly with the commencement of the Antarctic Cold Reversal in the southern hemisphere. Circa 12.5 ka, the Bølling-Allerød ended with the onset of the Younger Dryas, when numerous proxies indicate the northern hemisphere returned to near-glacial conditions; decreases in snow accumulation and high concentrations of dust in Greenland indicating colder, drier conditions (Alley et al., 1993), and negative excursions in $\delta^{18}O$ and $\delta^{15}N$ suggesting Greenland air temperature was up to 15° colder (Grootes and Stuiver, 1997; Severinghaus et al., 1998). At the same time, $\delta^{18}O$ and δD records from Antarctica exhibit a return to the deglacial warming trend (Johnsen et al., 1972; Steig et al., 1998; Blunier and Brook, 2001; Jouzel et al., 2001), signaling the end of the Antarctic Cold Reversal.

The question, given this anti-phased relationship between the Antarctic and Greenland deglaciation records is, does it follow that retreat of the other large ice sheets was also asynchronous between hemispheres? Certainly the LIS is located in the northern hemisphere closer to Greenland, but the LIS margin extended much farther south.

Interestingly, while the polar air temperature records do indeed appear to be asynchronous, records of smaller mid-latitude mountain glacier retreat suggest an earlier and synchronous mid-latitude warming. Schaefer et al. (2006) present a compilation of ^{10}Be exposure dates from moraines ranging 46.5°S to 47°N in New Zealand, Australia, Patagonia, Chile, the United States (Wyoming, Montana, Oregon, the Sierra Nevada range), and Switzerland, all of which place initial retreat between mean ages of 19.3 and

16.3 ka. This places the timing of mid-latitude glacial retreat closer to the "early" melting of Antarctica rather than Greenland.

Rinterknecht et al.(2006, 2007) similarly track initial retreat of the Fennoscandian ice sheet (FIS) through over 200 calibrated ^{10}Be and ^{14}C dates from seven suites of moraines between 52° and 60° latitude in southern Finland, Estonia, Latvia, Lithuania, Poland, and Belarus. These place the onset of FIS retreat at ~19.05 ka. As the FIS merged with the Barents and Kara ice sheets at their collective peaks at the height of the LGM (Rinterknecht et al., 2006), these two sheets are assumed to have similar retreat timing.

Research Questions

This project addresses two central questions: (1) Can a time frame be established for initial retreat of the Laurentide Ice Sheet at the end of the Last Glacial Maximum? (2) If so, how does the timing compare to other major deglacial records, including the other large ice sheets and mid-latitude mountain glaciers in both hemispheres?

Placing LIS retreat into this global perspective is critical to understanding the coherence of interhemispheric warming during the early deglaciation. If the LIS began to melt during the "early" phase of deglaciation, close in time to both the Antarctic and Fennoscandian ice sheets, as well as the smaller mid-latitude mountain glaciers in both hemispheres, it would suggest a more synchronous, coherent warming between hemispheres. This possibility would support atmospheric heat transport as a strong controlling factor on surface temperature between the hemispheres through increased summer insolation and greenhouse gas forcing.

If the initial LIS melt was closer in time to major initial Greenland warming at 14.67 ka, tracking the effects to the bipolar see-saw, it would support oceanic heat transport as the controlling factor on northern hemisphere surface temperatures and ice sheet ablation during deglaciation.

Approach: A Northern Gulf of Mexico Perspective

The questions discussed above were approached through analysis of deep-sea sediment cores taken from Orca Basin in the northern Gulf of Mexico. Paired stable isotope ($\delta^{18}O$) and trace metal (Mg/Ca) analysis was performed on the planktonic foraminifera *Globigerinoides ruber* (pink), as proxies for $\delta^{18}O$ of seawater and sea surface temperature, respectively.

The LIS had five major drainage routes for meltwater: the Mississippi River watershed to the south, the Hudson River watershed, St. Lawrence River watershed, and Hudson Strait between north Quebec and Baffin Island to the north and east, and drainage to the Arctic Ocean northwest of glacial Lake Agassiz (see Figure 1). At the peak of the LGM, the regions surrounding the Hudson River, Hudson Bay, St. Lawrence River, and Arctic northwest were locked up within the coverage of the ice sheet (Dyke et al. 2002) when the southern margin began melting. All early LIS meltwater should have been carried by the Mississippi River watershed, and ultimately delivered to the Gulf of Mexico. For the purpose of tracking early LIS meltwater, the northern Gulf of Mexico is therefore an ideal study site for geochemical proxies capable of tracing an influx of glacial freshwater from the Mississippi River drainage basin.

Stable isotope and trace metal proxies from Orca Basin have been used extensively to document deglacial LIS input to the Gulf of Mexico throughout the last glacial cycle. Leventer et al. (1982) made a study of $\delta^{18}O$ of the foraminifera *Globigerinoides ruber* as a salinity proxy in core EN32-PC6, covering almost 30 ka, in which they concluded LIS meltwater input to the Gulf of Mexico commenced between 18 and 16.5 ka. $\delta^{18}O$ values, however, are also affected by sea surface temperature (SST), and at the time of the study, Mg/Ca as an independent proxy for SST was not yet established. Age control was also based strictly on linear interpolation, assuming an age of zero at core top, one ^{14}C date at 3.915 ka, and one biostratigraphic event at the Y/Z boundary (~11 ka).

Flower et al. (2004) improved upon this data, presenting from the same core a record of paired Mg/Ca and $\delta^{18}O$ data on *G. ruber,* allowing the isolation of $\delta^{18}O$ of seawater, which, in turn, can be used to estimate salinity. The age control and temporal resolution of this study were insufficient to ascertain an accurate initial meltwater signal; sparse foraminifera between 19.2 and 17.2 ka allowed for only low resolution sampling (10 cm or less) in the lower portion of the core. And while age control was based on both new and previously published ^{14}C dates, only two were within the limits of Leventer et al.'s proposed early meltwater phase.

Williams et al. (2010) presented Mg/Ca data from Orca Basin core MD02-2550 on both *G. ruber* (white) and *G. ruber* (pink) at 1-cm resolution. Thirty-five ^{14}C dates provided comprehensive age control for evaluating deglacial Gulf of Mexico SST from 18.4 to 10.8 ka. The study provided a thorough picture of several abrupt climate changes recorded in the Gulf of Mexico, including the Younger Dryas, The lowest third of core

MD02-2550, however, was not evaluated. And while both pink and white *G. ruber* exhibit a warming trend from 18.4 until ~16.6 ka, it is unknown whether this warming trend leads, lags, or parallels the initial ablation of the LIS.

We aim to resolve this by performing identical paired Mg/Ca and $\delta^{18}O$ analysis on the lowest 300 cm of core MD02-2550, expanding on the work of Williams et al. (2010). The lower section of the core (~300 cm) extends from 18.4 ka back to 23.8 ka, well within the peak of the LGM. This study considers whether a time frame can be established, and proxy data generated to constrain initial melting of the LIS. The timing can then be compared to records for the Antarctic, Greenland, and Fennoscandian ice sheets, as well as the smaller mid-latitude mountain glaciers.

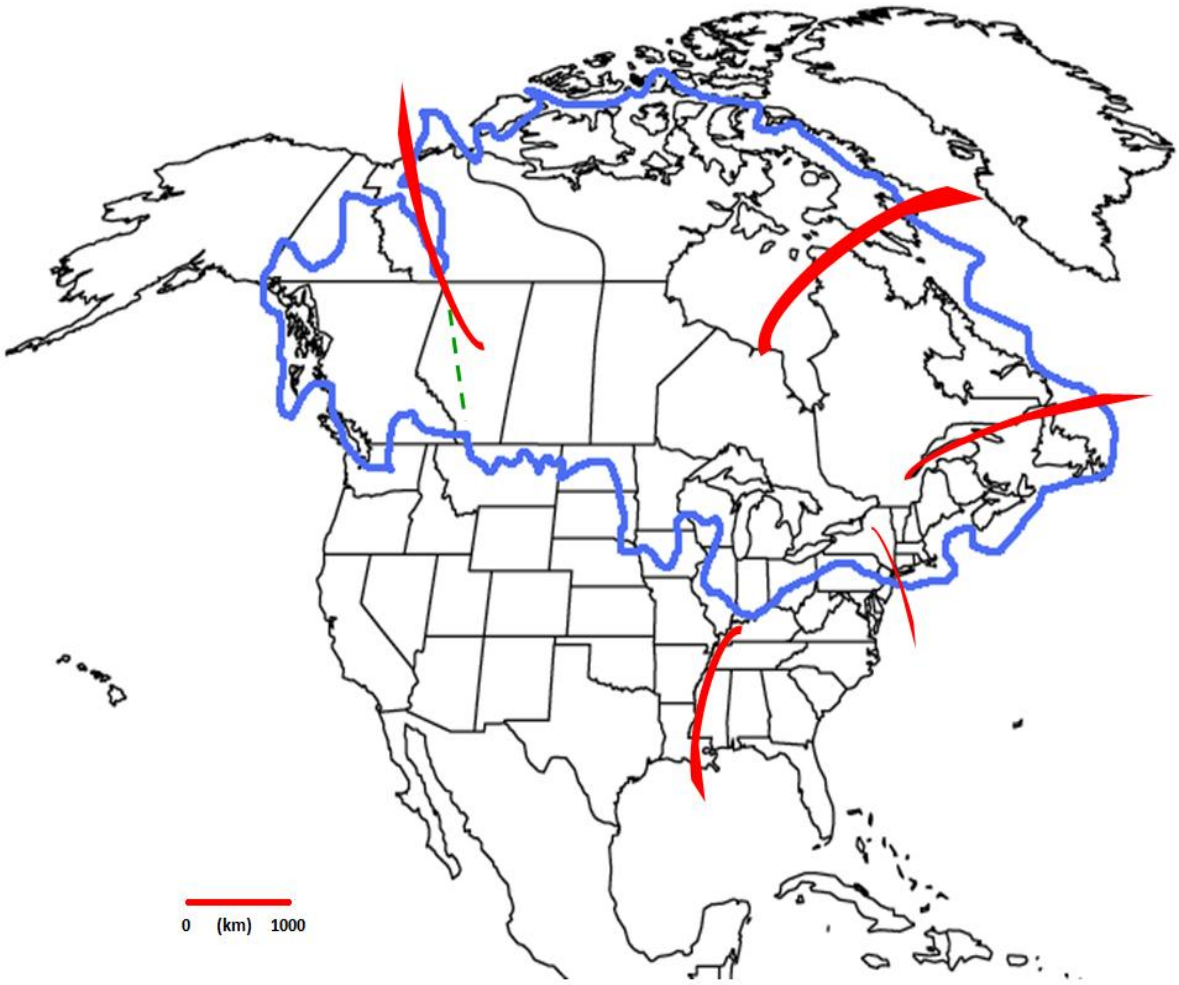

Figure 1. North American Laurentide Ice Sheet at maximum glacial extent, ~40° north latitude, circa 23 ka. Five major drainage routes, clockwise from top left are the Arctic Ocean drainage from glacial lake Agassiz, the Hudson Strait, the St. Lawrence River drainage basin, the Hudson River drainage basin, and the Mississippi River drainage basin. Image by the author.

METHODS

Study Site: Orca Basin

Orca Basin (26˚56.78' N, 91˚20.74' W; see Figure 2) is a 400 m^2 anoxic basin located in the continental slope 300 km south of the modern Mississippi Delta. The basin is 2.4 km deep, above the carbonate compensation depth, with a shallow (1 km) sill depth. A 200 m thick basal layer of hypersaline brine (salinity >250) limits the supply of oxygen, inhibiting the presence of benthic organisms to disturb the laminated sediments (McKee and Sinder, 1976). Combined with high accumulation rates of 30-50 cm/kyr, these aspects offer the potential for preserving an excellent high-resolution sediment record. Excellent carbonate preservation is supported by the presence of numerous carbonate planktonic foraminifera with intact spines, and aragonite pteropods with little to no dissolution.

Sampling

In July of 2002, the *R/V Marion Dufresne* recovered Calypso square gravity core MD02-2550 (25 cm^2, 9.08 m length) from Orca Basin at 2248 m water depth. Paired Mg/Ca SST and $\delta^{18}O$ data have previously been generated by Williams et al. (2010) up to 622 cm. The present study considers the lowest third of the core, covering the increment from 622 cm to the base of the core at 908 cm (ca. 18.36 – 23.88 ka).

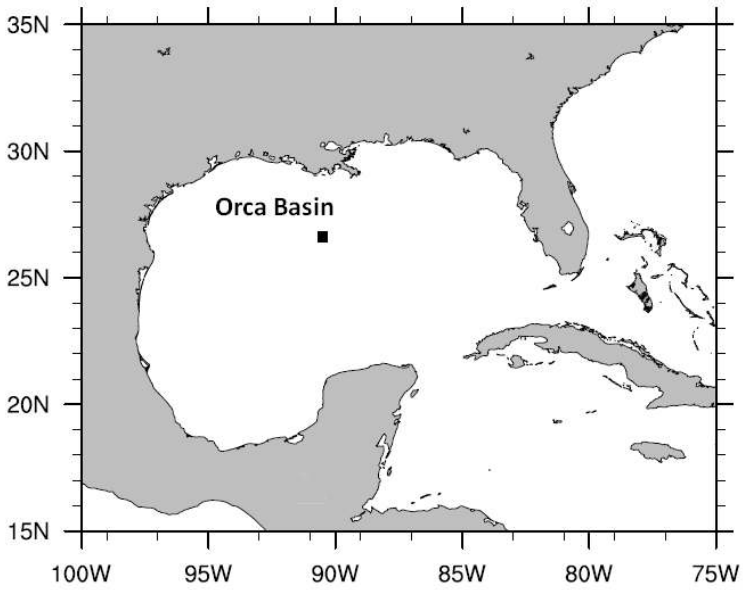

Figure 2. Map of the Gulf of Mexico showing the location of Orca Basin. Source: University Corporation for Atmospheric Research NCL (http://www.ncl.ucar.edu/Applications/ maponly.shtml).

Samples were freeze-dried prior to rinsing in deionized water over a 63-µm sieve. Seventy to one hundred (70-100) specimens of *Globigerinoides ruber* (pink) were picked from the 250-355 µm size fraction at 1-cm resolution throughout (see Appendix A,Table A1). 1 cm corresponds to approximately 20-30 years of sediment accumulation. Age control for the 18.36 – 23.88 ka interval was based on twelve accelerator mass spectrometer (AMS) ^{14}C dates generated at Lawrence Livermore National Laboratory, CA (see Table 1). Added to those from the interval covered by Williams et al. (2010), age control on core MD02-2550 is based on over forty-five AMS ^{14}C dates. Radiocarbon ages were converted to calendar years using the CALIB 6.0 program (discussed below) developed by Stuiver et al. (1998a).

Picked foraminifera from each interval were weighed, gently crushed between two glass plates under a binocular microscope to open test chambers where clays may

have accumulated, and homogenized to assure uniformity. 50-80 µg were allotted for stable isotope analysis, allowing additional material for replicates where possible. 300-400 µg were allotted for Mg/Ca analysis.

For stable isotope analysis, samples were rinsed in methanol and sonicated to remove adhering particles, then dried in an oven overnight at ~35°C. Data were generated on a ThermoFinnigan DeltaPlus XL stable isotope ratio mass spectrometer (SIRMS) coupled to a Kiel-III carbonate preparation device with a long-term analytical precision of ±0.06‰ for $\delta^{18}O_{calcite}$. Samples were measured against six NBS-19 standards for every run. Average sample precision based on 54 replicate samples is ±0.21‰.

For Mg/Ca analysis, samples were cleaned following a four-step procedure (Barker et al.,2003). Each aliquot was rinsed four times in Milli-Q water and twice in trace metal clean methanol to remove adherent clays, cleaned in a buffered hot (90°C) solution of hydrogen peroxide (H_2O_2) and 0.1 M sodium hydroxide (NaOH) to remove organic material, and weak (0.001 M) nitric acid leach (HNO_3) to remove any remaining adsorbed contaminants.

Immediately before analysis, samples were dissolved in 0.75 N HNO_3, and centrifuged at 5000 rpm for 5 minutes to force any remaining clay out of suspension. 350 µL of the resulting solution was then transferred to 17x1000 mm polyethylene tubes, and diluted with an appropriate amount of 2% HNO_3 to bring each sample to a target 25 ppm calcium concentration. Mg/Ca ratios were generated on an Agilent Technologies 7500cx inductively coupled plasma mass spectrometer (ICP-MS). Average precision based on 48 replicates is ±0.17 mmol/mol Mg/Ca. Both instruments are located at the College of Marine Science, University of South Florida.

Material

Globigerinoides ruber is a symbiotic dinoflagellate-bearing spinose planktonic foraminifera dwelling in the mixed layer of sub-tropical to tropical waters (Bé 1977; Nürnberg et al., 1996a; Dekens et al., 2002; Tedesco et al., 2009). Its relative abundance makes it a common species for both modern and paleo low-latitude geochemical studies with Mg/Ca and $\delta^{18}O$ (e.g. Dekens et al., 2002; Anand et al., 2003; Flower et al., 2004; Hill et al. 2006; Williams et al. 2010).

The species has two color variants: pink and white, one of which (white) is further divided into two morphological variants (Wang, 2000; Steinke et al., 2005). All of these variants are present in the Gulf of Mexico (Tedesco et al., 2009). *G. ruber* (pink) calcifies from the surface to a depth of about 25 meters, while *G. ruber* (white) may calcify from the surface down to a depth of 50 meters (Wang, 2000; Anand et al., 2003; Steinke et al., 2005). *G. ruber* (pink) is a spring-to-summer-dominant species, prevalent during the spring in the northern Gulf of Mexico (Tedesco et al., 2009). It therefore records surface conditions weighted toward the warmer season (Anand et al., 2003).

G. ruber (pink) were selected for the purpose of this study, as summer is the point when melting is likely to have occurred during the period of maximum glaciation. In addition, *G. ruber* (pink) was simply more abundant than *G. ruber* (white) in almost all intervals sampled from 622-908 cm, often by up to three times as much material.

Age Model

Twelve accelerator mass spectrometer (AMS) ^{14}C dates on monospecific *G. ruber* samples between 622 and 908 cm (see Table 1) were converted to calibrated calendar

year ages using the CALIB probability distribution program (http://calib.qub.ac.uk/calib/calib.html), originally written at the Quaternary Isotope Lab at the University of Washington (Stuiver and Reimer, 1986). Allowing that marine environments are exposed to ^{14}C at a different rate than subaerial environments, CALIB version 6.0 applies the most current radiocarbon to calendar age calibration for marine samples (Marine09), with a time-dependent ocean reservoir correction of ~405 years (Reimer et al., 2009).

Table 1. Twelve accelerator mass spectrometry (AMS) ^{14}C dates on monospecific *G. ruber* converted to calendar ages using the CALIB 6.0 program (Stuiver et al., 1998a).

Core Depth (cm)	^{14}C Ages (Years)	^{14}C Error (Years)	Calibrated Age (ka)
650	16345	50	18.91
681	16450	60	19.40
700	16500	50	19.73
725	17470	60	20.27
750	18480	60	20.89
775	18480	70	21.44
803	18790	70	22.05
825	19380	70	22.45
851	19710	70	22.89
871	19750	70	23.23
903	20340	60	23.75
908*	19290	70	22.46

*Sample 908 was not included in the age model, due to chronological inconsistency.

A weighted curve fit smoothed 15% was applied to the AMS ^{14}C dates against core depth to convert to calendar age (see Figure 3). Error bars reflect a 2 standard deviation (2-sigma) error in calibration. Temporal resolution based on calculated ages is ~19.64 years per sample from 622 cm to 649 cm, 15.94 years/sample from 650 – 680 cm, 16.86 years/sample from 680 – 699 cm, 21.84 years/sample from 700 – 724 cm, 24.60 years/sample from 725 – 748 cm, 21.99 years/sample from 749 – 802, 17.11 years/sample from 802 – 901, and 26.30 years/sample throughout the core bottom.

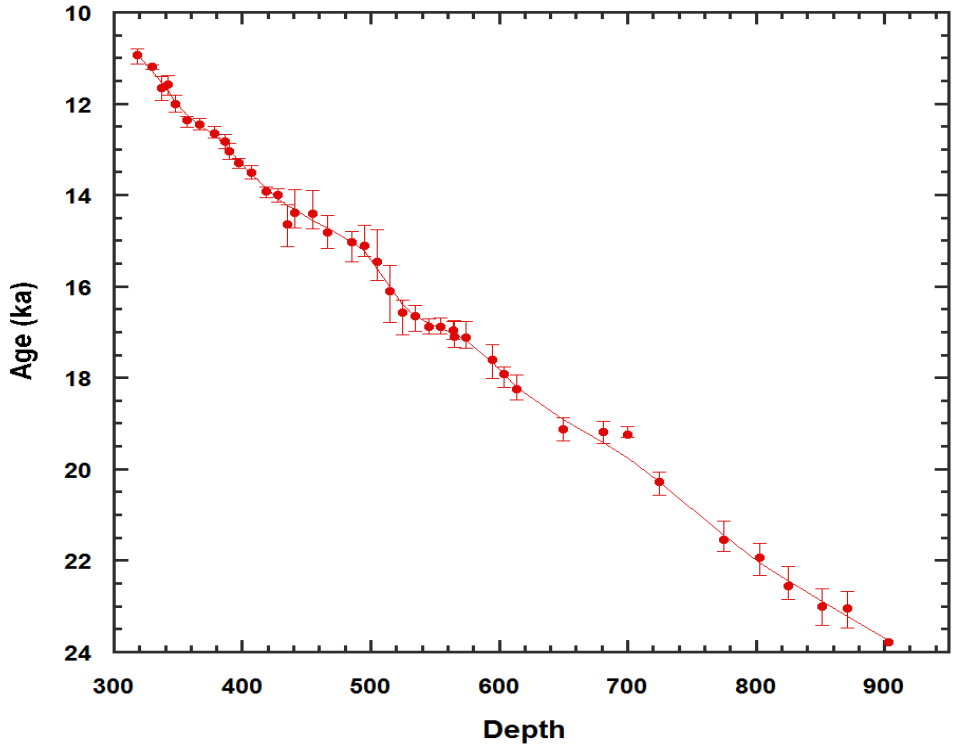

Figure 3. Age model for core MD02-2550, based on 45 AMS ^{14}C dates from monospecific *G. ruber*. 12 dates are within the interval covered by this study; the remaining dates extend through the upper portion of the core analyzed by Williams et al. (2010).

Mg/Ca

The incorporation of magnesium into a foraminifera's test is a biologically mediated thermodynamic reaction in which divalent magnesium (Mg^{++}) is substituted into the calcite lattice as temperature rises (Oomori et al., 1987; Nürnberg et al., 1996a; Lea et al., 1999; Dekens et al., 2002). Unlike $\delta^{18}O$, temperature appears to be the single dominant factor controlling Mg/Ca, except under extreme circumstances. Holding temperature constant, surface salinity changes of over 10‰ are required for pronounced changes in Mg/Ca (Ferguson et al., 2008; Arbuszewski et al., 2010), whereas a 1°C change in temperature will change Mg/Ca by ~9.0±0.3% (in nine species analyzed by Anand et al., 2003). Provided the influencing factors can be either excluded or

constrained, foraminiferal Mg/Ca may thus be used as a proxy for paleo-sea surface temperature (Nürnberg et al., 1996a; Hastings et al., 1998).

Mg/Ca is appealing not only as a proxy for SST independent of $\delta^{18}O$, but also because when measured in the same samples as $\delta^{18}O$, it can be used to subtract the temperature component of $\delta^{18}O$ in foraminifera, allowing the isolation of the ice volume and salinity effects (e.g. Lea et al., 2000; Flower et al., 2004; Hill et al., 2006). SST was calculated from the exponential calibration from Anand et al. (2003):

$$Mg/Ca = B * \exp (A*T)°C.$$

Based on a six-year sediment trap time series in the Saragasso Sea, Anand et al. (2003), derived an equation specifically for *G. ruber* (pink), assigning pre-exponential and exponential values of B = 0.38(±0.1) and A = 0.090, respectively.

The resulting equation is very similar to that employed by Dekens et al. (2002), but the Dekens formula Mg/Ca = 0.38*exp (0.09*(SST - 0.61 (core depth km)) is meant to address the effects of dissolution in the deep sea. As the sill of Orca Basin is above the lysocline, this is unnecessary for our core. The formula for pink *G. ruber* used by Anand et al (2003), was rearranged from Mg/Ca = 0.38 *exp (0.090*SST(°C)) to SST(°C) = ln (MgCa/0.381(±0.01))/0.090. This solves for SST at the time of calcification, with an accuracy of ±1.2°C.

$\delta^{18}O$: Sea Surface Temperature

The $\delta^{18}O$ signal incorporated into foraminiferal calcium carbonate test ($\delta^{18}O_{calcite}$) reflects a combination of the isotopic effects of sea surface temperature (SST), and the $\delta^{18}O$ value of the ambient seawater ($\delta^{18}O_{sw}$) from which the test precipitated (Epstein et

al., 1953; Ruddiman and Mix, 1984; Mix, 1987; Bemis et al., 1998). $\delta^{18}O_{sw}$, in turn, is a function of salinity and ice volume.

Mg/Ca as an independent proxy allows the SST component of $\delta^{18}O_{calcite}$ to be isolated. For this study, the high-light equation developed for symbiont-bearing *O. universa* cultures by Bemis et al. (1998) was used: $T(°C) = 14.9(\pm0.1) - 4.80(\pm0.8) * (\delta^{18}O_{calcite} - \delta^{18}O_{sw})$.

Temperature was obtained from the Mg/Ca ratios (discussed above) in all samples with sufficient quantity of material to run both Mg/Ca and $\delta^{18}O$ analysis. The remaining value is the $\delta^{18}O_{sw}$ signal, reflecting an amalgamation of salinity and ice volume effects. Both the Bemis equation and the raw data generated on the SIRMS are expressed on the Vienna PeeDee Belemnite scale (VPDB). For compatibility with all subsequent calculations, a constant of 0.27‰ was added to convert $\delta^{18}O_{sw}$ to the Vienna standard mean ocean water scale (VSMOW).

$\delta^{18}O_{sw}$: Ice Volume

The formation of large, sustained, isotopically depleted ice sheets over periods of geological time has the effect of isotopically enriching sea water during glacial intervals (Emiliani, 1955; Shackleton and Opdyke, 1973; Ruddiman and Mix, 1984; Mix, 1987; Sharp, 2006). Mix (1987) further observed that despite numerous local influences such as local freezing or melting effects, bioturbation, closed basins and carbonate dissolution, a striking similarity exists among glacial planktonic and benthic $\delta^{18}O$ records around the world. Mix concluded the explanation is a change in ice volume, which could potentially affect waters in multiple basins on a global scale over thousands of years.

In order to isolate the effects of salinity on $\delta^{18}O_{sw}$ therefore, a correction must be made for ice volume. Ruddiman and Mix (1984) noted that this correction may not be entirely straightforward. A linear relationship between ice volume and $\delta^{18}O_{sw}$ assumes that $\delta^{18}O$ of the ice sheet is constant from initial formation to maximum extent (and subsequently, initial melting to late deglaciation). They argued it is much more probable for $\delta^{18}O$ in the accumulating snow to become progressively more depleted as the ice sheet grows larger.

This is due in part to the effects of colder temperatures (both from a decrease in air temperature and increase in glacier height), an increase in altitude (meteoric $\delta^{18}O$ decreases ~0.26‰ per 100 m elevation), and decrease in latitude as the ice sheet expands (– 0.5‰ for every 10° north; Sharp, 2006). These caveats, however, cannot be further quantified. For the remainder of this study, ice volume-corrected $\delta^{18}O_{sw}$ will therefore be considered a first-order salinity indicator.

To correct for ice volume, projected calendar age for each sample was modeled against a sea-level history curve from Barbados (Fairbanks, 1989) to calculate sea level at each sample interval. Using modern sea level as a zero point, the correction of 0.083‰ per 10 meters of sea level change was applied. The 0.083‰ value is based on a global average change in $\delta^{18}O_{sw}$ of 1‰ (Schrag et al., 2002) divided by 120 meters of sea level rise since the LGM (Fairbanks, 1989). The residual ice volume-corrected signal ($\delta^{18}O_{sw\text{-}ivc}$) was then considered as representing solely the part of the isotope signal affected by sea surface salinity.

$\delta^{18}O_{sw\text{-}ivc}$: Salinity

At low latitudes in the modern ocean, $\delta^{18}O_{sw\text{-}ivc}$ and salinity exhibit a linear relationship (Schmidt et al., 1999), but the specifics of the slope and intercept depend on the low salinity end-member. Using plausible high and low salinity and $\delta^{18}O_{sw\text{-}ivc}$ end-members and assuming a linear relationship at the time of the LGM, a simple mixing model can be constructed, from which salinity can be estimated (see Figure 4).

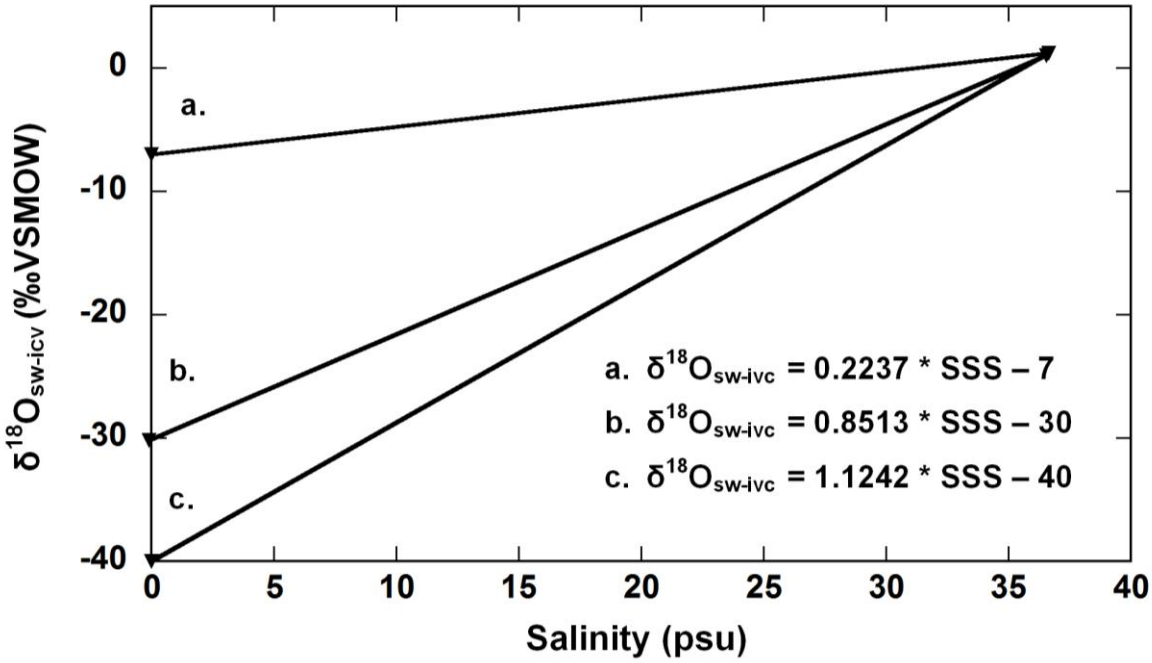

Figure 4. Mixing model constructed for the Gulf of Mexico expressing linear relationship between $\delta^{18}O_{sw\text{-}ivc}$ and salinity. Slope and intercept for each scenario are determined by one plausible high salinity end-member and three low salinity end-members.

Like Ruddiman and Mix's argument for the non-constant $\delta^{18}O$ value of ice sheets (1984), Nürnberg et al. (2008) noted, in their estimates of Desoto Canyon SSS in the northeastern Gulf of Mexico, that the modern linear relationship for $\delta^{18}O_{sw}$ and salinity might not necessarily hold through time. LIS inflow to the Gulf of Mexico very likely changed over deglaciation via changes in $\delta^{18}O$ of LIS meltwater (possible values range

-20‰ to -42‰, as suggested by Dansgaard and Tauber, 1969; Fairbanks 1989; Ruddiman and Mix, 1984; Flower et al., 2004), and probably via changes in precipitation as the climate became warmer. Salinity reconstruction therefore has an additional uncertainty due to changing end-member composition over time.

For this study, a high salinity end-member of S = 36.65 psu, $\delta^{18}O_{sw\text{-}ivc}$ = 1.2‰ (Fairbanks et al., 1992) was considered appropriate. From this point, three possible low salinity end-members were then projected: -7‰ as the value for modern Mississippi River water (Ortner et al., 1995), and two extremely low values of -30‰ and -40‰, considered probable values of LIS meltwater. The modern Mississippi River $\delta^{18}O$ value of -7‰ yields a very low slope of 0.2, while the two LIS estimates yield slopes of 0.9 and 1.1, respectively (see Figure 4; Appendix A2).

RESULTS

Mg/Ca

In the 622 to 908 cm section of core MD02-2550, Mg/Ca exhibits a mean value of 3.12 ± 0.23 mmol/mol (see Figure 5), equivalent to 23.37 ± 0.83°C, based on the equation for pink *G. ruber* by Anand et al. (2003). This is compares to a modern mean summer SST of ~27.26 ±0.5°C. Furthermore, throughout the interval, Mg/Ca exhibits recurring variability of ~0.5 mmol/mol (~1.7°C from the equation of Anand et al., 2003). These oscillations occur consistently, on approximately a 10-cm scale, and while they appear to increase in magnitude from ~850 - 900 cm, this may be due to less sample material and poorer temporal resolution toward the bottom of the core.

$\delta^{18}O$: Sea Surface Temperature & Ice-Volume

Raw $\delta^{18}O$ signals of foraminiferal tests exhibit a mean value of -1.27 ± 0.62‰ on the VPDB scale (see Figure 5). At all sampling intervals containing sufficient material to run both stable isotope and trace metal analysis (>400µg), independent SST from Mg/Ca analysis was used to remove the SST component of $\delta^{18}O$ (see Methods), solving for $\delta^{18}O_{sw}$ (also in Figure 5). A 0.27‰ constant was then added to convert $\delta^{18}O_{sw}$ to the VSMOW scale for all subsequent calculations. $\delta^{18}O_{sw}$ prior to ice-volume correction has a mean value of 0.72‰ (VSMOW). Like the Mg/Ca signal, variations of ~1.5‰ occur on roughly a 10-cm scale, although this is not as well constrained, as many samples toward the lower part of the core lacked sufficient material to run both Mg/Ca and $\delta^{18}O$ analysis.

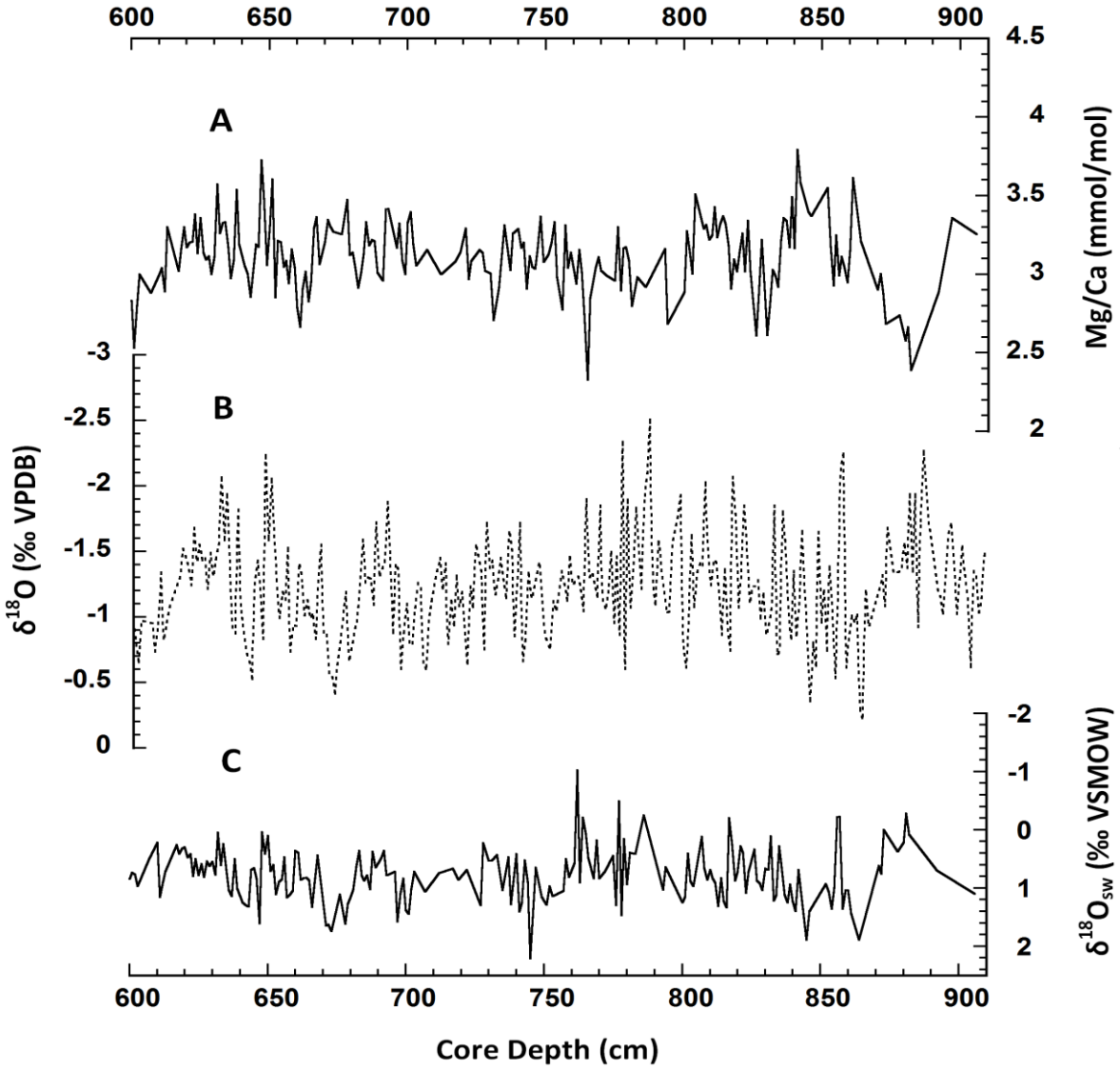

Figure 5. Raw data from Orca basin core MD02-2550 vs depth (cm): (A) Mg/Ca (mean 3.12 ± 0.23 mmol/mol) and (B) Raw $\delta^{18}O$ of the foraminiferal tests (mean -1.27 ± 0.62‰ VPDB scale), and (C) $\delta^{18}O_{sw}$ signal with the temperature component removed, converted to the VSMOW scale (mean 0.72‰; see text for methods and calculations). Data are based on 1-cm sampling resolution, except where an interval lacked sufficient material for geochemical analysis.

Modeling a projected calendar age for each sample against Fairbanks' 1989 coral sea level history curve (see *Age Model* and *Ice Volume* sections of Methods) yields a total change in sea level of –29.56 meters over the 622-908 cm section of the core (18.36 - 23.88 ka). This translates to a total change in $\delta^{18}O_{sw}$ of 0.24‰ over the same section.

Applying the Schrag et al. (2002) ice volume correction of 0.083‰ $\delta^{18}O$ (VSMOW) per 10 meters of sea level change to each of the samples yields an ice-volume corrected mean $\delta^{18}O_{sw\text{-}ivc}$ value of –0.27‰ during the LGM. This compares to a modern mean of 1.2‰ (Fairbanks et al., 1992). This residual $\delta^{18}O_{sw\text{-}ivc}$ can then be considered in terms of salinity.

$\delta^{18}O_{sw\text{-}ivc}$: Salinity

Salinity data based on three possible low end-members reveal excursions mirror-imaging those of $\delta^{18}O_{sw\text{-}ivc}$, with high salinity values corresponding to the most isotopically enriched seawater, and low salinity at isotopically depleted intervals. It is worth noting that the more negative low end-member zero-intercepts with steeper slopes (representing a greater the difference from modern $\delta^{18}O_{sw\text{-}ivc}$), produce much smaller changes in salinity. By contrast, using the modern Mississippi River water $\delta^{18}O$ value of -7‰ as an end-member, the linear equation yields salinity shifts as great as 6-12‰ (see Figure 6).

Modern Gulf of Mexico SSS typically ranges 32.6 to 35.6‰ on a seasonal basis (Fairbanks et al., 1992; Levitus and Boyer, 1994). By comparison, the two plausible end-member isotopic compositions of -30‰ and -40‰, plausible isotopic compositions for the LIS (Dansgaard and Tauber, 1969; Ruddiman and Mix, 1984; Fairbanks, 1989) produce very small shifts of generally <1‰ throughout the LGM. The difference between the mean salinity value based on the -40‰ end-member (35.27‰) and that based on the -30‰ end-member (34.92‰) is only 0.35‰.

Therefore, even accounting for Ruddiman and Mix's argument for the isotopic composition of the LIS changing as the ice sheet grew or melted, this model suggests that even a change of 10‰ in the parent ice sheet as the end-member source accounts for only small changes in Gulf of Mexico salinity during the LGM, perhaps even within error of the calculated $\delta^{18}O_{sw\text{-}ivc}$.

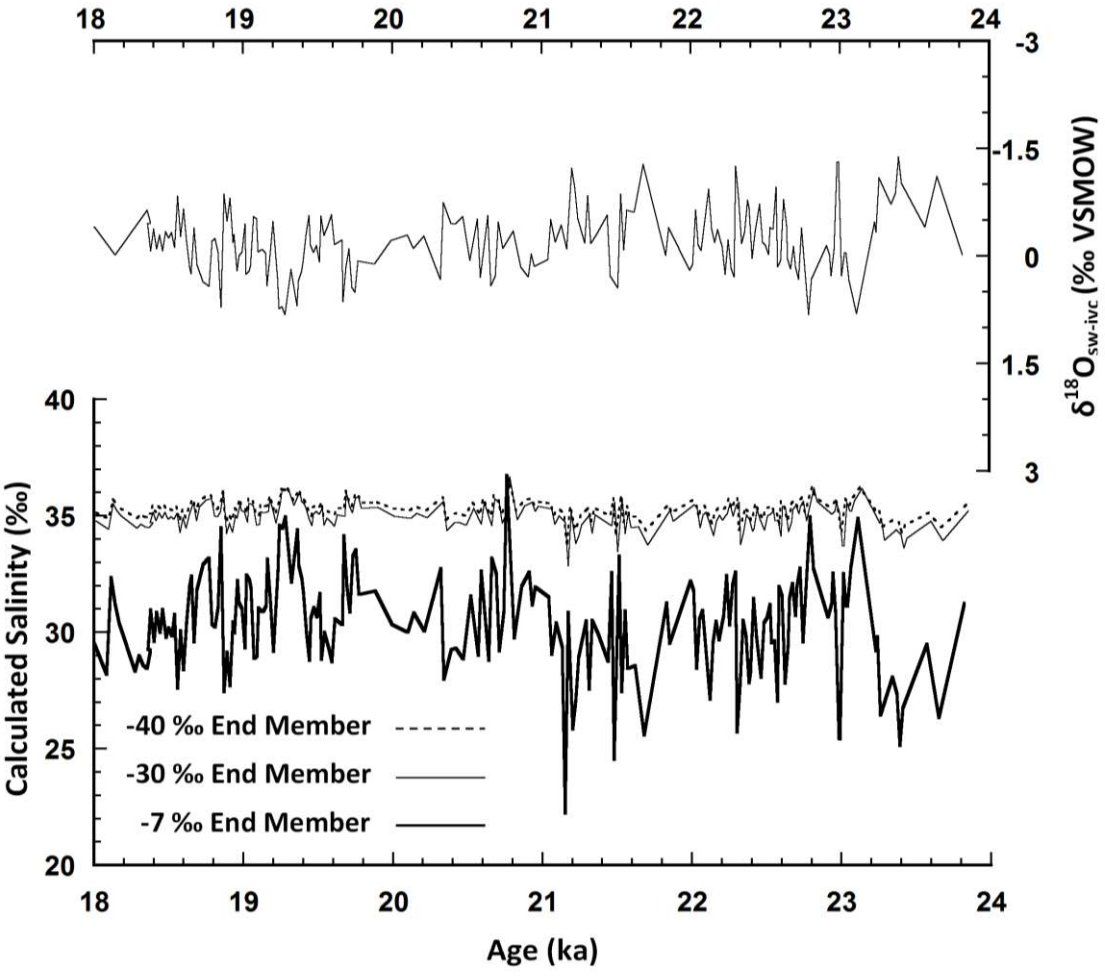

Figure 6. Calculated salinity based on three possible low salinity end-members for Laurentide Ice Sheet meltwater, and a high salinity end-member of S = 36.65 psu, $\delta^{18}O_{sw\text{-}ivc}$ = 1.2‰ (from Fairbanks et al., 1992). LGM Gulf of Mexico $\delta^{18}O_{sw\text{-}ivc}$ record is shown for reference. An end-member of -7‰ yields extremely large shifts in salinity. -30 and -40‰ are much more probable values for meltwater end-members, and yield very small salinity shifts

DISCUSSION

In order to fully assess the proxy records from Orca Basin from a Gulf of Mexico perspective, paired data from interval 622-908 cm were combined with the data of Williams et al. (2010), also from core MD02-2550, creating a continuous record based on *G. ruber* (pink) from 311 to 908 cm, corresponding to 10.73 – 23.86 ka. This combined record encompasses the middle to latter LGM, the initial deglaciation, the Oldest Dryas, the Bølling-Allerød warm interstadial, Younger Dryas, and early Holocene epoch (see Figure 7). The compiled core MD02-2550 records are compared to air temperature records from the northern hemisphere, based on Greenland Ice Sheet Project 2 (GISP 2) $\delta^{18}O$ in ice, and from the southern hemisphere, based on δD from the European Project for Ice Coring in Antarctica (EPICA) Dome C (see Figure 7).

Sea Surface Temperature During the LGM

Throughout the LGM, *G. ruber* (pink) maintains a mean value of 23.37 ± 0.83°C for the Gulf of Mexico surface waters (see Figure 7). The raw LGM Mg/Ca mean of 3.12 mmol/mol from this study further corroborates with the mean Mg/Ca values of 3.18 mmol/mol observed in Orca Basin at low temporal resolution between 21 and 19 ka by Flower et al. (2004).

While *G. ruber* is a summer-dominant species (Tedesco et al., 2009), the data from this study and that of Flower et al. (2004) indicate a significantly cooler SST for the

Gulf of Mexico during the LGM than has been previously estimated. The Climate Long-Range Investigation, Mapping and Prediction (CLIMAP) project (1976; 1981) estimated a mean August SST for the Gulf of Mexico during the LGM was 26°C, or just over 1°C cooler than present mean of 27.26°C (CLIMAP project members, 1976; CLIMAP project members, 1981; Anderson and Webb, 1994; Crowley, 2000).

CLIMAP's estimate for Gulf of Mexico SST, however, was based strictly on faunal assemblages. Following CLIMAP's original report, an abundance of paleoproxies including $\delta^{18}O$ recorded in foraminifera (e.g. Kennett and Shackleton, 1975; Crowley and Matthews, 1983), $\delta^{18}O$ recorded in coral (e.g. Fairbanks and Matthews, 1977; Fairbanks et al., 1989; Guilderson et al., 1994), Sr/Ca recorded in corals (e.g. Guilderson et al., 1994), algal Uk_{37} saturation index of long-chain alkenones (e.g. Jasper and Gagosian 1989; Ohkouchi et al., 1994), and paleo vegetation records (e.g Webster and Streten., 1978) have suggested LGM temperatures ranging 1° to almost 10° lower than present in the low-latitude Atlantic.

The magnitude of tropical and subtropical SST changes since the LGM is critical to understanding the sensitivity of the climate system to glacial forcings, especially since SST boundary conditions frequently serve as the basis for climate reconstruction models (Crowley, 2000, MARGO project members, 2009). Reconciling these proxies has therefore been a controversial effort, but one of monumental importance.

The LGM SST reconstruction in this study falls within what Crowley (2000) describes as a "mid-range sensitivity" (3.0-2.5°C change in the tropical to sub-tropical regions). Crowley suggests this range is reconcilable with changes in modeled atmospheric lapse rate and a stronger pole-to-tropics cooling gradient, while still allowing

the persistence of tropical and subtropical plankton biota. A stronger low-latitude cooling than CLIMAP predicted suggests the subtropical latitudes were in fact highly sensitive to the changes brought on by glacial conditions.

Sea Surface Temperature During the Deglacial Period

The LGM mean of 23.37 °C is not, in fact, the lowest SST observed in this study. One striking feature of the Mg/Ca record occurs at ~18.4 ka, with an abrupt drop of almost 2°C, from a mean LGM SST of 23.37 °C to a mean of 21.75°C. This cold period lasts from 18.4 ka until ~17.8 ka. At 17.8 ka, it begins a sustained warming trend that persists until the end of the Bølling-Allerød.

The magnitude of SST change from LGM is best illustrated in combination with the data of Williams et al. (2010; see Figure 7). Onset of the cold snap occurs very near the junction where data from the two studies meet, which raises the question of whether one set of foraminifera was more properly cleaned, analyzed, and processed. However, the youngest few SST data points from this study (ranging 22.7 to 21.4°C) are in agreement with the oldest data points from Williams et al. (2010), whose lowest core section ranges 22.5 to 21.1°C. Additionally, fresh samples from 622 to 670 cm were picked for Mg/Ca at all intervals where enough material could be put together for a second analysis. Replicate SST values matched the first analysis within a range of 0.02°C to 0.52°C.

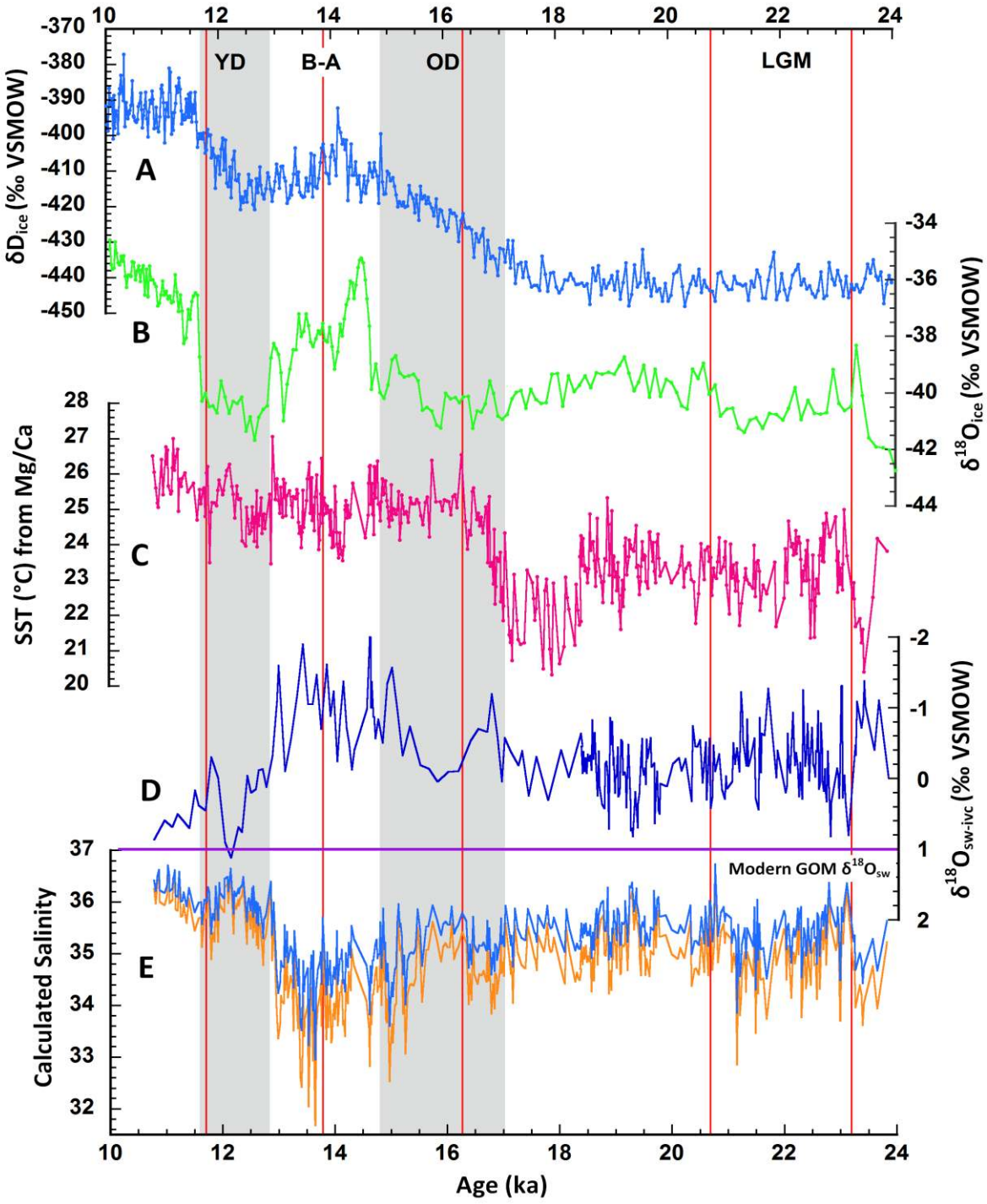

Figure 7. Compiled deglacial proxy records from 10.73 – 23.88 ka. (A) δD from Antarctica EPICA Dome C, (B) $\delta^{18}O$ from Greenland GISP 2, (C) Gulf of Mexico SST based on Mg/Ca from Williams et al. (2010) and this study, Gulf of Mexico $\delta^{18}O_{sw\text{-}ivc}$ from Williams et al. (2010) and this study, with modern GOM $\delta^{18}O_{sw}$ included for reference, and (E) salinity based on two end-members (-30‰ in orange, -40‰ in blue), calculated from $\delta^{18}O_{sw\text{-}ivc}$. These are compared to five re-advances of the LIS based on moraine exposure (red lines; Lowell et al., 1999).

Recovery from this cold snap circa17.8 ka falls within timing of the retreat of the mid-latitude mountain glaciers (16.3-19.3 ka), although the latter begins earlier. Mass balance of smaller glaciers is highly sensitive to changes in precipitation and small changes in temperature during the summer melting season (Schaefer et al., 2006); the larger LIS may have withstood a forcing mechanism toward melting for slightly longer.

The SST warming trend at 17.8 ka lies within the warming trend recorded in Antarctic air temperature (~19-17 ka), but whereas the Antarctic warming record was a gradual rise over a two-thousand year period, Gulf of Mexico SST increases much more sharply (almost 4°C in a thousand years). However, this is still an early temperature increase relative to the onset of the Bølling-Allerød warm period as recorded in Greenland ice (~14.67 ka).

At present, we do not have a satisfactory explanation for the anomalous cold snap. *G. ruber* (pink) is a summer-dominant species; one explanation might simply be a record of colder summers. However, the seasonal cooling must have persisted for almost a thousand years. Decreased insolation is not a possible mechanism for this, since, between 20 and 16 ka, incoming solar radiation in the northern hemisphere was rising slowly (Berger and Loutre, 1991). Furthermore, the mid-latitude mountain glaciers (46.5° S to 47°N) lay within comparable latitude to the LIS margin (~40°N). As the mountain glaciers are highly sensitive to summer temperatures, and evidence from Schaefer et al. (2006) suggests the glaciers were in synchronous retreat during this time frame, this explanation is unlikely.

Another explanation might be that, since *G. ruber* is a surface-dwelling species, it may be recording a cold glacial freshwater lens, delivered by the Mississippi River. To

achieve this cold water lens effect, glacial water must have maintained its cold temperature the entire course of its journey from the glacial margin at 40° north to Orca Basin at 26° north. Modeling this scenario would require knowledge or plausible estimation of Mississippi River volume and discharge, ambient air temperature, estimated heat loss over the distance covered, and the volume and temperature values of significant tributaries feeding the Mississippi River en route. It would also need to be able to reconcile why, if SST represents a surge of glacial freshwater, did $\delta^{18}O_{sw\text{-}ivc}$ and corresponding salinity not decrease to correspondingly lower values until several thousand years later, during the Bølling-Allerød (see Figure 7)?

If this were in fact the case, then the initial marker for initial LIS meltwater should be considered the "drop" at 18.4 ka, rather than the sustained recovery. This would place initial ablation at 18.4 ka. This date also lies within the timing of mid-latitude mountain glacier retreat (16.3-19.3 ka), although the mountain glacier retreat still begins earlier.

$\delta^{18}O_{sw\text{-}ivc}$

Unlike Mg/Ca-derived SST, the mean $\delta^{18}O_{sw\text{-}ivc}$ value of –0.27‰ (VSMOW) exhibits little to no noticeable increase toward modern mean (~1.2‰) at all during the LGM. Seven negative excursions of almost 1‰ and five positive excursions, also of almost 1‰ are observed in the 622-908 cm interval (see Figure 7).

With the SST component subtracted out, the two factors controlling the $\delta^{18}O$ seawater value can arguably both be attributed to the dynamics of the ice sheet: changes in global ice volume, and changes in $\delta^{18}O$ based on parent meltwater drainage during ablation. Lowell et al. (1999) explore the importance of ablation – specifically ablation

rate – on the millennial scale, as the primary control on ice sheet dynamics. They also suggest ablation rate may be an indicator of the link between climate and ice sheet dynamics. Radiocarbon dating of moraines in the midwestern United States, reflecting the time the ice sheet reached its terminal position, suggest eight pulses or short retreats of the LIS southern margin, after which it re-advanced. Each of these pulses occurs at, or just before a short (millennial scale) but relatively rapid warming recorded in GISP2 ice cores from the Greenland Summit.

Five of these pulses from terminal position lie within the chronological range of this study, and have been graphed for comparison (see Figures 7). Four of the LIS re-advances, as noted by Lowell et al. (1999) at 11.6 ka, 13.8 ka, 16.3 ka, and 23.4 ka), correspond to relatively large (>1‰) negative excursions in $\delta^{18}O_{sw\text{-}ivc}$. One (20.7 ka) lies in a relatively stadial period with no major excursions.

These dates observed by Lowell et al. are interesting to compare to the Gulf of Mexico $\delta^{18}O_{sw}$ record for several reasons, not least among which is because, unlike GISP2, the MD20-2550 core allows the comparison of LIS melting pulses to a proxy that is actually recording the LIS meltwater. It is also interesting to note that the LIS margin appears to have been fluctuating in tandem with Gulf of Mexico $\delta^{18}O$, influenced by meltwater, on a millennial scale.

Furthermore, if, as Lowell et al. (1999) suggest, there is a possible linkage of climate dynamics between the LIS margin pulses and Greenland air temperature on the millennial time scale, then $\delta^{18}O_{sw}$ from the MD02-2550 core offers an independent source of evidence to test this. If the pulses coincide with a negative excursion in $\delta^{18}O$ in both Orca Basin (26˚56.78’ N, 91˚20.74’ W) and the Greenland Summit (72^{o} 36’ N, 38^{o}

30’ W), it might support the linkage, despite warming recorded in SST not mirroring Greenland at all on the longer deglacial time scale. Since ablation rate is a function of net loss through melting and sublimation over net accumulation, the negative excursions and minor retreats likely reflect periods when warmer summers caused higher melting than winter accumulation could make up for.

The concept of a largely synchronous termination of the LGM would require a redistribution of heat on a geologically short time scale. Increase in summer insolation is widely considered the initial forcing; incoming summer (July) solar radiation in the northern hemisphere at 65° N rose from ~410 W m^{-2} at 20 ka to over 450 W m^{-2} by 16 ka (Berger and Loutre, 1991). Summer radiation 65° S peaked at 450 W m^{-2} near 20 ka, and while it decreased until ~15 ka, the incoming value never fell below 440 W m^{-2}. But insolation changes were quite slow, so strong positive feedback mechanisms are needed to explain the observed rapid responses in regional temperature change.

Salinity

Low-latitude salinity was clearly lower than present across the globe during the LGM (GLAMAP members, 2003). Our high-resolution $\delta^{18}O_{sw}$-derived salinity estimates from the Gulf of Mexico corroborate existing data from this region. Both of the extreme high end-members -30‰ and -40‰, when applied to the linear $\delta^{18}O_{sw}$-SSS model, produce LGM salinities with means of 34.8 and 35.2, respectively (see Figure 7; Appendix A2). These salinity estimates are in agreement with the salinity 35 – 35.4 estimated for the northern Gulf of Mexico south of the Mississippi delta by Schäfer-Neth and Paul (2003) using data from the German Glacial Atlantic Ocean Mapping project

(GLAMAP members, 2003). These values are at least 1 unit lower than modern Gulf of Mexico salinity.

Interestingly, salinity exhibits no major "pulse" suggesting a single initial LIS melting event. These low salinities in fact persist through the LGM, and well into the early deglaciation phase SST. Like the GLAMAP data, our estimates are significantly lower than the modern SSS mean of 36.5‰, warranting the question of what influences would affect $\delta^{18}O_{sw}$ to create a steady-state lower salinity environment in the northern Gulf of Mexico during the LGM.

Salinity in the modern ocean is largely a balance of evaporation vs. precipitation, plus river runoff in some nearshore areas. A major control on increased moisture and precipitation in the tropical Atlantic lies in the position of the Intertropical Convergence Zone, or ITCZ (Barry and Chorley, 1992). However, the modern latitudinal extent of the ITCZ during the boreal summer is 10°N at maximum (Waliser and Gautier, 1993). Moreover, as one effect of large ice sheets at high latitudes is to induce rapid air cooling, progressing to mid and lower latitudes via the northeasterly trade winds and inducing colder SST "fronts" where the ITCZ forms, the ITCZ in glacial times was both weakened and pushed farther south from its modern mean position (e.g. Chiang et al., 2003; Chiang and Bitz, 2005; Broccoli et al., 2006; Nürnberg et al., 2008; Schmidt et al., 2011), associated with a reduced Atlantic meridional overturning. The ITCZ is therefore unlikely to have had direct influence on Gulf of Mexico precipitation during the LGM.

Cold stadial periods in the Atlantic are associated with a reduced production of North Atlantic Deep Water, NADW, leading to both weaker and shallower circulation of water masses in the Atlantic (e.g. Duplessy et al., 1988; Curry et al., 1988; Shin et al.,

2003; Schmidt et al., 2004). Based on this, Nürnberg et al. (2008) have made a case for an indirect effect of the ITCZ on Gulf of Mexico SSS during glacial intervals. As the ITCZ shifted south, SSS in the tropical Atlantic increased, partly due to enhanced evaporation, but also due to strong prevailing northeasterly winds over the Caribbean and a weakening of the Gulf Stream associated with NADW circulation. Reduced circulation should also have weakened the Florida Loop Current, carrying less warm, salty tropical water into the Gulf, and exporting less "fresh" meltwater from it, through the Straits of Florida, to the Gulf Stream. This would maintain a glacial Gulf of Mexico with lower SST and less saline SSS conditions.

This is an intriguing hypothesis, but a source is still needed for the initial "colder, fresher" conditions in the Gulf of Mexico. Gulf of Mexico $\delta^{18}O_{sw}$ could be influenced by the isotopic composition of meltwater, mixing with the Mississippi River (Leventer et al., 1982; Ruddiman and Mix, 1984; Nürnberg et al. 2008). It could also be influenced by the amount of evaporation vs. precipitation, both over the sea, and over the portions of the continent contributing to the Mississippi River drainage basin. A higher continental precipitation factor would increase the volumetric amount of freshwater the Mississippi was delivering to the Gulf, which would, in turn, also influence the values of $\delta^{18}O_{sw}$.

Numerous proxies, including aeolian dust concentrations in ice cores from both the northern and southern hemispheres (e.g. Petit et al., 1990), increased salinity in the Atlantic Warm Pool (e.g. Schmidt et al., 2004), and a weakening of the ITCZ over the equatorial Atlantic and Pacific (e.g. Chaing et al., 2003) suggest that parts of the globe during the LGM were significantly drier than present.

Kim et al. (2003), however, used a coupled climate model, observed proxies, and a paired atmosphere-mixed layer ocean slab model to simulate the LGM global hydrologic cycle. This suggested that the markedly dry LGM conditions are strongest in three distinct bands: (1) the northern hemisphere from 50-70°N, associated with the presence of the large ice sheets in Europe, Greenland and North America; (2) proximal to the equator, associated with a weak ITCZ, and (3) over 70° S, associated with the Antarctic ice sheet. In contrast, simulated displacement of the jet stream by the LIS showed an increase of precipitation over the southern portion of North America between 20° and 40°N, and an increase in Mississippi River discharge of over $42x10^3$ m^3 s^{-1}, more than 3 times the modern discharge rate (Kim et al., 2003).

Laurentide Ice Sheet Ablation

Taken together, several of these hypotheses may begin to explain the data observed during the LGM in Orca Basin. A steady rise in incoming solar radiation (for July) may have been recorded in Mg/Ca in the summer-dominant *G. ruber*. Increased precipitation in the continental front-land south of the LIS margin could have combined with initial pulses of extremely depleted glacial meltwater as the southern margin fluctuated on the millennial scale before a full LIS retreat began.

These two factors together would have created an isotopically light Mississippi River discharge, which may have also been carrying substantial volumes of water at a high discharge rate. Ample quantities of isotopically light, fresh water injected into northern Gulf of Mexico could potentially drive SSS to lower than modern values, maintained throughout the LGM early deglaciation by a weaker Loop Current and a

steady supply of glacial meltwater as long as the Mississippi River remained the major LIS drainage route. The low-salinity signal persisted well into the Younger Dryas (see Figure 7), suggesting that, rather than a single major onset of ablation, the LIS was in fact melting and re-advancing along the southern margin throughout the LGM.

Exactly how much each individual factor influenced the geochemical proxy record is beyond the scope of this study. However, the similar timing of SST recovery to the time of mid-latitude glacier retreat on the deglacial scale, the parallel between Gulf of Mexico $\delta^{18}O_{sw\text{-}ivc}$, LIS marginal pulses and Greenland air temperature on the millennial scale, as well as the possible influence of enhanced precipitation following displacement of the jet stream by the LIS, suggest atmospheric heat and moisture transport as the strong controlling factor on early deglaciation between the hemispheres, augmented by redistribution of heat by ocean circulation.

The mean $\delta^{18}O_{sw\text{-}ivc}$ value recorded by the summer-dominant *G. ruber* appears to continue at steady state well into the early deglacial phase of the Gulf of Mexico. As enhanced precipitation, early pulses of LIS melting, and the higher discharge rates associated with them would very likely have begun on a seasonal basis, a comparative high-resolution study of *G. ruber* white (in progress) recording a more year-round signal in the same interval will be extremely beneficial for a more comprehensive reconstruction of LIS deglaciation recorded in Gulf of Mexico sediments.

CONCLUSIONS

Mg/Ca and $\delta^{18}O$ analysis of the planktonic foraminifera *Globigerinoides ruber* (pink) at a high (1-cm) sampling resolution are used to isolate northern Gulf of Mexico SST and $\delta^{18}O_{sw}$ at the transition from the Last Glacial Maximum to the early stages of deglaciation. Twelve AMS ^{14}C dates provide good age constraints (18.36-23.88 ka) and indicate a high sediment accumulation rate in Orca Basin. A longer record is constructed by combining the present study with previous work from core MD02-2550 (Williams et al., 2010), which can be compared to deglacial records from other large ice sheets.

Mg/Ca-derived SST exhibits a mean of 23.37 ± 0.83°C from 23.88 to 18.4 ka, almost 4° colder than present. This SST calculation is also lower than originally predicted by the CLIMAP model, implying a higher degree of low-latitude sensitivity to climate forcings under glacial conditions. At 18.4 ka, SST exhibits a sharp drop to a mean of 21.75°C. This cold snap persists until 17.8 ka, when a sustained recovery begins. The warming trend in the Gulf of Mexico occurs early relative to the onset of the Bølling-Allerød warm period, much earlier than major deglacial warming in Greenland (~14.67 ka), and somewhat later than the initial ice sheet retreat based on glacial moraine dating in Fennoscandia (~19.09 ka). This SST warming weakly resembles that of Antarctica (17-19 ka), but does not parallel it.

$\delta^{18}O_{sw\text{-}ivc}$ persists in stadial conditions well into the deglacial period, in fact well into the Younger Dryas, with a mean of –0.27‰ (compared to a modern mean of 1.2‰). Several abrupt millennial-scale negative excursions of over 1‰ appear to correlate with

pulses of LIS retreat and re-advance based on continental moraine dating, indicating terminal positions of the southern LIS margin. This suggests a link between meltwater input and ice sheet retreat. These pulses also compare to abrupt negative excursions in $\delta^{18}O$ from the Greenland GISP2 ice core. The similarity between Greenland $\delta^{18}O$ trend and Gulf of Mexico $\delta^{18}O_{sw\text{-}ivc}$ trend on short time scales also suggests a link, requiring a rapid distribution of heat across the northern hemisphere.

A sustained increase in incoming solar radiation of 40 W m^{-2} between 20 and 16 ka in the northern hemisphere may be recorded in Mg/Ca in the summer-dominant *G. ruber* after 17.8 ka, although it does not explain the anomalous cold snap. It may, however, have contributed to warmer summers, triggering several small-scale ablations at the southern margin of the LIS, accounting for the negative $\delta^{18}O_{sw\text{-}ivc}$ excursions in both the Gulf of Mexico and Greenland.

A simple mixing model based on plausible low salinity end-member $\delta^{18}O$ values of the LIS also suggests the Gulf of Mexico surface water salinities were between 34.8 and 35.2, significantly fresher than present mean annual salinity of 36.5.

Pulses of meltwater at the oscillating margin, possibly in combination with increased precipitation south of the LIS margin resulting in creased Mississippi River discharge, may account for this.

Based on this study, a single major "initial deglacial pulse" of Laurentide Ice Sheet ablation is not apparent. The initial research question addressed at the beginning of this project therefore remains unanswered. The dynamics of the southern LIS margin appear to have been intriguingly complex, requiring additional data analysis in future.

Evaluation of the *G. ruber* (white) variety, not biased toward the summer season, may provide new insight to the Mg/Ca and $\delta^{18}O_{sw}$ record of the northern Gulf of Mexico as study of core MD02-2550 continues. Spectral analysis will be performed on SST and $\delta^{18}O_{sw\text{-}ivc}$ to evaluate the "oscillations" for true periodic signals. $\delta^{18}O_{sw}$ records will further be compared to additional terrestrial records of LIS margin fluctuation (Lowell & Curry, in prep) as they become available.

REFERENCES

Alley, R.B., 2003. The Younger Dryas cold interval as viewed from central Greenland. Quaternary Science Reviews 19: 213-226.

Alley, R.B., Meese, D.A., Shuman, C.A., Gow, A.J., Taylor, K.C., Grootes, P.M., White, J.W.C., Ram, M., Waddington, E.D., Mayewski, P.A., Zielinski, G.A., 1993. Abrupt increase in Greenland snow accumulation at the end of the Younger Dryas event. Nature 362: 527-529.

Anand, P., Elderfield, H., Conte, M.H., 2003. Calibration of Mg/Ca thermometry in planktonic foraminifera from a sediment trap time series. Paleoceanography 18(2): 1050, doi:10.1029/2002PA000846.

Anderson, D.M., Webb, R.S., 1994. Ice-age tropics revisited. Nature 367: 23-24.

Anderson, J.B., Shipp, S.S., Lowe, A.L., Wellner, J.S., Mosola, A.B., 2002. The Antarctic ice sheet during the Last Glacial Maximum and its subsequent retreat history: a review. Quaternary Science Reviews 21: 49-70.

Arbuszewski, J., deMenocal, P., Kaplan, A., Farmer, E.C., 2010. On the fidelity of shell-derived $\delta^{18}O_{seawater}$ estimates. Earth and Planetary Science Letters 300(3-4): 185-196.

Barry, R.G., Chorley, R.J., 1992. Atmosphere, weather and climate. London: Routledge.

Bé, A.W.H.,1977. An ecological, zoogeographic and taxonomic review of recent planktonic foraminifera, *in* Ramsay, A.T. eds., Oceanic micropaleontology. London: Academic Press.

Bemis, B.E., Spero, H.J. Bijma, J., Lea, D.W., 1998. Reevaluation of the oxygen isotopic composition of planktonic foraminifera: Experimental results and revised paleotemperature equations. Paleoceanography 18(2): 150-160.

Berger, A., Loutre, M.F., 1991. Insolation values for the climate of the last 10 million years. Quaternary Science Reviews 10(4): 297-317.

Blunier, T., Brook, E.J., 2001. Timing of millennial-scale climate change in Antarctica and Greenland during the last glacial period. Science 291:109-112.

Broccoli, A.J., Dahl, K.A., Stouffer, R.J., 2006. Response of the ITCZ to northern hemisphere cooling. Geophysical Research Letters 33: L01702, doi: 10.1029/2005GL024546.

Clark, P.U., Alley, R.B., Pollard, D., 1999. Northern hemisphere ice sheet influences on global climate change. Science 286: 1104-111.

Clark, P.U., Dyke, A.S., Shakun, J.D., Carlson, A.E., Clark, J., Wohlfarth, B., Mitrovica, J.X., Hostetler, S.W., McCabe, A.M., 2009. The last glacial maximum. Science 325: 710-714.

Clark, P.U., Mix, A.C., 2002. Ice sheets and sea level of the last glacial maximum. Quaternary Science Review 21: 1-7.

CLIMAP Project Members, 1976. The surface of ice-age Earth: quantitative geologic evidence is used to reconstruct boundary conditions for the climate 18,000 years ago. Science 191: 1131-1137.

CLIMAP Project Members, 1981. Seasonal reconstructions of Earth's surface at the last Glacial Maximum. Geological Society of America Chart Ser., MC-36.

Chiang, J.C.H., Biasutti, M., Biasutti, D.S., 2003. Sensitivity of the Atlantic intertropical convergence zone to the last glacial maximum boundary conditions. Paleoceanography 18(4): 1094 doi:10.1029/2003PA000916.

Chiang, J.C.H., Bitz, C.M., 2004. Influence of high latitude ice cover on the marine intertropical convergence zone. Climate Dynamics 25: 477-496

Crowley, T.J., 1992. North Atlantic deep water cools the southern hemisphere. Paleoceanography 7(4): 489-497.

Crowley, T.J., 2000. CLIMAP SSTs revisited. Climate Dynamics 16: 241-255.

Crowley, T.J., Matthews, R.K., 1983. Isotope-plankton comparisons in a late Quaternary core with a stable temperature history. Geology 11: 275-278.

Curry, W.B., Duplessy, J.C., Labeyrie, L.D., Shackleton, N.J., 1988. Changes in the distribution of $\delta^{13}C$ of deep water ΣCO_2 between the Last Glaciation and the Holocene. Paleoceanography 3(3): 317-341, 1988 doi:10.1029/ PA003i003p00317.

Dansgaard, W., Tauber, H., 1969. Glacier oxygen 18 content and Pleistocene ocean temperatures. Science 166: 499-502.

Denton, G.H., Anderson, R.F., Toggweiler, J.R., Edwards, R.L., Schaefer, J.M., Putnam, A.E., 2010. The last glacial termination. Science 328: 1652-1656.

Denton, G.H., Hughes, T.J., 1981. The Last Great Ice Sheets. New York: Wiley.

Denton, G.H., Hughes, T.J., 2002. Reconstructing the Antarctic Ice Sheet at the Last Glacial Maximum. Quaternary Science Reviews 21: 193-202.

Duplessy, J.C., Shackleton, N.J., Fairbanks, R.J., Labeyrie, L., Oppo, D., Kallel, N.,1988. Deepwater source variations during the last climatic cycle and their impact on the global deepwater circulation. Paleoceanography 3(3): 343-360,doi:10.1029/ PA003i003p00343.

Dyke, A.S., Andrews, J.T., Clarke, P.U., England, J.H., Miller, G.H., Shaw, J., Veillette., J.J., 2002. The Laurentide and Innuitian ice sheets during the Last Glacial Maximum. Quaternary Science Review 21: 9-31.

Dyke, A.S., Prest, V.K., 1987. Late Wisconsinian and Holocene history of the Laurentide ice sheet. Géographie physique et Quaternaire 41(2): 237-263.

Emiliani, C., 1955. Pleistocene temperatures. Journal of Geology 63: 538-578.

Epstein, S., Buchsbaum, H.A., Lowenstam, H.A., Urey, H.C., 1953. Revised carbonate-water isotopic temperature scale. Geological Society of America Bulletin 64: 1315-1325.

Fairbanks, R.G., 1989. A 17,000-year glacio-eustatic sea level record: influence of glacial melting rates on the Younger Dryas event and deep ocean circulation. Nature 342: 637-642.

Fairbanks, R.J., Matthews, R.K., 1978. The marine oxygen isotope record in Pleistocene coral, Barbados, West Indies. Quaternary Research 10:181-196.

Ferguson, J.E., Henderson, G.M., Kucera, M., Rickaby, R.E.M., 2008. Systematic change of foraminiferal Mg/Ca ratios across a strong salinity gradient. Earth and Planetary Science Letters 265: 153-166.

Flower, B.P., Hastings, D.W., Hill, H.W., Quinn, T.M., 2004. Phasing of deglacial warming and Laurentide Ice Sheet meltwater in the Gulf of Mexico. Geology 32(7): 597-600.

GLAMAP project members: Sarnthein, M., Gersonde, R., Niebler, S., Pflaumann, U., Spielhagn, R., Thiede, J., Wefer, G., Weinelt, M., 2003. Overview of Glacial Atlantic Ocean Mapping (GLAMAP 2000). Paleoceanography 18(2): 1030, doi:10.1029/2002PA000769.

Grootes, P.M., Stuiver, M., 1997. Oxygen 18/16 variability in Greenland snow and ice with 10^{-3} to 10^{5}-year time resolution. Journal of Geophysical Research 102(C12): 26,455 – 26,470, doi:10.1029/97JC00880.

Guilderson, T.P., Fairbanks, R.G., Rubenstone, J.L., 1994. Tropical temperature variations since 20,000 years ago: modulating interhemispheric climate change. Science 263(5147): 663-665, doi 10.1126/science.263.5147.663.

Hastings, D.W., Russell, A., Emerson, S.,1998. Foraminiferal magnesium in G. sacculifer as a paleotemperature proxy. Paleoceanography, 13:161-169.

Hill, H.W., Flower, B.P., Quinn, T.M., Hollander, D.J., Guilderson, T.P., 2006. Laurentide Ice Sheet meltwater and abrupt climate change during the last glaciation. Paleoceanography 21 PA1006, doi:10.1029/2005PA001186.

Jasper, J.P., Gagosian, R.B., 1989. Alkenone molecular stratigraphy in an oceanic environment affected by glacial freshwater events. Paleoceanography 4(6): 603-614.

Johnsen, S.J., Dansgaard, W., Clausen, H.B., Langway, C.C., 1972. Oxygen isotope profiles through the Antarctic and Greenland ice sheets. Nature 235: 229-234.

Jouzel, J., Masson, V., Cattani, O., Falourd, S., Stievenard, M., Stenni, B., Longinelli, A., Johnsen, S.J., Steffensen, J.P., Petit, J.R., Schwander, J., Souchez, R, Barkov., N.I., 2001. A new 27 ky high resolution East Antarctic climate record. Geophysical Research Letters 28(16): 3199-3202.

Lambeck., K., 1995. Constraints on the Late Weichselian ice sheet over the Barents Sea from observations of raised shorelines. Quaternary Science Reviews 14(1): 1-16.

Lea, D.W., Mashiotta, T.A., Spero, H.J., 1999. Controls on magnesium and strontium uptake in planktonic foraminifera determined by live culturing. Geochimica et Cosmochimica Acta 63: 2369-2379, doi:10.1016/S0016-7037(99)00197-0.

Lea, D.W., Pak, D.K., Spero, H.J., 2000. Climate impact of late Quaternary equatorial Pacific sea surface temperature variation. Science 8(289): 1719-1724, doi: 10.1126/science.289.5485.1719.

Leventer, A., Williams, D.F., Kennett, J.P., 1982. Dynamics of the Laurentide ice sheet during the last deglaciation: evidence from the Gulf of Mexico. Earth and Science Letters 59: 11-17.

Levitus, S., Boyer, T.P., 1994. World Ocean Atlas 1994: US-Department of Commerce, NOAA Atlas NEDIS, National Oceanic and Atmospheric Administration, Silver Spring, MD.

Liccardi, J.M., Clark, P.U., Jenson, J.W., Macayeal, D.R., 1998. Deglaciation of a soft-bedded Laurentide ice sheet. Quaternary Science Reviews 17: 427-448.

Kennett, J.P., Shackleton, N.J., 1975. Laurentide ice sheet meltwater recorded in Gulf of Mexico deep-sea cores. Science 188: 147-150.

Knies, J., Vogt, C., Matthiessen, J., Nam, S.-I., Ottesen, D., Rise, L., Bargel, T., and Eilertsen, R.S., 2007. Re-advance of the Fennoscandian Ice Sheet during Heinrich Event 1. Marine Geology 240: 1-18.

Knutti, R., Flückiger, J., Stocker, T.F., Timmerman, A., 2004. Strong hemispheric coupling of glacial climate through freshwater discharge and ocean circulation. Nature 430(7002): 851-856.

Manabe, S., Broccoli, A.J., 1985b. The influence of continental ice sheets on the climate of an ice age. Journal of Geophysical Research 90: 2167-2190.

MARGO Project Members, 2009. Constraints on the magnitude and patterns of ocean cooling at the Last Glacial Maximum. Nature Geoscience 2: 127-132, doi: 10.1038/NGEO411.

Mix, A.C., 1987. The oxygen-isotope record of glaciation, *in* Ruddiman, W.F., and Wright, H.E. Jr., eds., North America and adjacent oceans during the last deglaciation: Boulder, Colorado, Geological Society of America, The Geology of North America v. K-3.

Mix, A.C., Bard, E., Schneider, R., 2001. Environmental processes of the ice age: land, ocean, glaciers (EPILOG). Quaternary Science Reviews 20: 627-657.

Monnin, E., Indermüle, A., Dällenbach, A., Flückiger, J., Stauffer, B., Stocker, T.F., Raynaud, D., Barnola, J-M., 2001. Atmospheric CO_2 concentrations over the last glacial termination. Science 291: 112-114.

Nakada, M., Lambeck, K., 1988. The melting history of the late Pleistocene Antarctic ice sheet. Nature 333(5): 36-40.

Nürnberg, D., Bijma, J., Hemleben, C., 1996. Assessing the reliability of magnesium in foraminiferal calcite as a proxy for water mass temperatures. Geochimica et Cosmochimica Acta 60(5): 803-814.

Nürnberg, D., Ziegler, M., Karas, C., Tiedemann, R., Schmidt, M., 2008. Interacting Loop Current variability and Mississippi River discharge over the past 400 kyr. Earth and Planetary Science Letters 272: 278-289 doi:10.1016/j.epsl.2008.04.051.

Ohkouchi, N., Kawamura, K., Nakamura, T., Taira, A., 1994. Small changes in the seas surface temperature during the last 20,000 years: molecular evidence from the western tropical Pacific. Geophysical Research Letters 21(20): 2207-2210.

Oomori, T., Kaneshima, H., Maezato, Y., 1987: Distribution coefficient of Mg^{2+} ions between calcite and solution at 10-50°C. Marine Chemistry 20: 327-336.

Ortner, P.B., Lee, T.N., Milne, P.J., Zika, R.G., Clarke, M.E., Podesta, G.P., Swart, P.K., Tester, P.A., Atkinson, L.P., Johnson, W.R., 1995. Mississippi River flood waters that reached the Gulf Stream. Journal of Geophysical Research 100: 13595-13601.

Pollard, D., Thompson, S.L., 1997. Climate and ice-sheet mass balance at the last glacial maximum from the GENESIS version 2 global climate model. Quaternary Science Reviews 16(8): 841-863, doi:10.1016/S0277-3791(96)00115-1.

Petit, J.-R., Jouzel, J., Raynaud, D., Barkov, N.I., Barnola, J.-M., Basile, I., Benders, M., Chappellaz, J., Davisk, M., Delaygue, G., Delmotte, M., Kotlyakov, V.M., Legrand, M., Lipenkov, V.Y., Lorius, C., Pépin, L., Ritz, C., Saltzmank, E, Stievenard, M. 1999. Climate and atmospheric history of the past 420,000 years from the Vostok ice core, Antarctica. Nature 399: 429-436.

Petit, J.-R., Mourner, L., Jouzel, J, Korotkevich, Y.S., Kotlyakov, V.I., Lorius, C., 1990. Palaeoclimatological and chronological implications of the Vostok core dust record. Nature 343: 56-58.

Reimer, P.J., Baillie, M.G.L., Bard, E., Bayliss, A., Beck, J.W., Blackwell, P.G., Bronk Ramsey, C., Bucks, C.E., Burr, G.S., Edwards, R.L., Friedrich, M., Grootes, P.M., Guilderson, T.P., Hajdas, I., Heatons, T.J., Hogg, A.G., Hughen, K.A., Kaiser, K.F., Kromer, B., McCormac, F.G., Manning, S.W., Reimer, R.W., Richards, D.A., Southon, J.R., Talamo, S., Turney, C.S.M., van der Plicht, J., Weyhenmeyer, C.E., 2009. INTCAL09 and MARINE09 radicarbon age calibration curves, 0-50,000 years. Radiocarbon 51(4): 1111-1150.

Rinterkneckt, V.R., Clark, P.U., Raisbeck, G.M., Yiou, F., Bitinas, A., Brook, E.J., Marks, L., Zelčs, V., Lunkka, J.-P., Pavlovskaya, I.E., Piotrowski, J.A., Raukas, A. 2006. The last deglaciation of the southeastern sector of the Scandinavian ice sheet. Science 311: 1449-1452.

Rinterkneckt, V.R., Pavlovskaya, I,E., Clark, P.U., Raisbeck, G.M., Yiou, F., Brook, E.J., 2007. Timing of the last deglaciation in Belarus. Boreas 36: 307-313, doi 10.1080/03009480601134694.

Ruddiman, W.F., Mix, A.C., 1984. Oxygen-isotope analysis and Pleistocene ice volumes. Quaternary Research 21: 1-20.

Schaefer, J.M., Denton, G.H., Barrell, D.J.A., Ivy-Ochs, S., Kubik, P.W., Andersen, B.G., Hillips, F.M., Lowell, T.V., Schlüchter, C., 2006. Near-synchronous interhemispheric termination of the last glacial maximum in mid-latitudes. Science 312: 1510-1513.

Schäfer-Neth, C., Paul., A., 2003. The Atlantic Ocean at the Last Glacial Maximum: 1. objective mapping of the GLAMAP sea-surface conditions, *in* Wefer, G., Mulitza, S., Ratmeyer, V., eds., 2003, The South Atlantic in the Late Quaternary: reconstruction of material budgets and current systems. Springer-Verlag: Berlin, Heidelberg, New York, Tokyo: 531-548.

Schmidt, M.W., Spero, H.J., 2011. Meridional shifts in the marine ITCZ and tropical hydrologic cycle over the last three glacial cycles. Paleoceanography 26: PA1206, doi:10.1029/2010PA001976.

Schrag, D.P., Adkins, J.F., McIntyre, K., Alexander, J.L., Hodell, D.A., Charles, C.D., McManus, J.F., 2002. The oxygen isotopic composition of seawater during the last glacial maximum. Quaternary Science Reviews 21: 331-342.

Severinghaus, J.P., Sowers, T., Brook, E.J., Alley, R.B., Bender, M.L., 1998. Timing of abrupt climate change at the end of the Younger Dryas interval from thermally fractionated gases in polar ice. Nature 391: 141-146.

Shackleton, N.J., Opdyke, N.D., 1973. Oxygen isotope and paleomagnetic stratigraphy of equatorial Pacific core V28-V39: Oxygen isotope temperatures and ice volumes on a 10^5 and 10^6 year scale. Quaternary Science Reviews 3: 39–55.

Sharp, Z., 2006. Principles of Stable Isotope Geochemistry. Upper Saddle River, NJ: Prentice Hall.

Shin, S.-I., Liu, Z., Otto-Bliesner, B.L., Kutzbach, J.E., Vavrus, S.J., 2003. Southern sea-ice control of the glacial North Atlantic thermohaline circulation. Geophysical Research Letters 30(2): 1096, doi:10.1029/2002GL015513.

Siegert, M.J., Dowdeswell, J.A., Melles, M., 1999. Late Weichselian glaciation of the Russian High Arctic. Quaternary Research 52: 273-285.

Steig, E.J., Brook, E.J., White, J.W.C., Sucher, C.M., Bender, M.L., Lehman, S.J., Morse, D.L., Waddington, E.D., Clow, G.D., 1998. Synchronous climate changes in Antarctica and the north Atlantic. Science 282: 92-95.

Stocker, T.F., 1998. The see-saw effect. Science 282 (5386): 61-62.

Stuiver, M., Grootes, P.M., 2000. GISP2 oxygen isotope ratios. Quaternary Research 53: 277-284.

Stuiver, M., Reimer, P. J., 1986. A Computer-Program for Radiocarbon Age Calibration. Radiocarbon, 28(2B): 1022-1030.

Stuiver, M., Reimer, P.J., Bard, E., Beck, J.W., Burr, G.S., Hughen, K.A. Kromer, B., McCormac, G., van der Plicht, J., Spurk, M., 1998a. INTCAL98 radiocarbon age calibration, 24,000-0 cal BP. Radiocarbon 40: 1041–1083.

Tedesco, K.A., Spear, J.W., Tappa, E., Poore, R.Z., 2009. Seasonal flux and assemblage composition of planktic foraminifera from the northern Gulf of Mexico. U.S. Geological Survey, Open File Report 2009-1293, 19 pp.

Waliser, D.E., Gautier, C., 1993. A satellite-derived climatology of the ITCZ. Journal of Climate (United States) 6(11): 2162-2174.

Webster, P.J., Streten, N.A., 1978. Late Quaternary ice age climates of tropical Austalasia: interpretations and reconstructions. Quaternary Research 10: 279-309.

Williams, C., Flower, B.P., Hastings, D.W., Guilderson, T.P., Quinn, K.A., Goddard, E.A., 2010. Deglacial abrupt change in the Atlantic Warm Pool: a Gulf of Mexico perspective. Paleoceanography 25: PA4221, doi:10.1029/2010PA001928.

APPENDIX A

Data for Core MD02-2550 from 622-908 cm

APPENDIX A

Data for Core MD02-2550 from 622-908 cm

Table A1. Samples for Core MD02-2550 from 622-908 cm (18.36-23.88 ka): Raw Mg/Ca and $\delta^{18}O$ converted to SST and $\delta^{18}O_{sw\text{-}ivc}$.

Depth (cm)	Age (ka) from model	Mg/Ca (mmol/mol)	SST (C°)	$\delta^{18}O$ ‰ (VPDB)	$\delta^{18}O_{sw}$‰ (VSMOW)	Sea Level Change (m)	$\delta^{18}O_{sw\text{-}ivc}$‰ (VSMOW)
622	18.36	2.88	22.47	-1.68	0.17	-105.08	-0.70
623	18.38	2.62	21.42	-1.42	0.21	-105.20	-0.66
624	18.40	2.91	22.59	-1.55	0.33	-105.32	-0.55
625	18.42	3.36	24.18	-1.43	0.78	-105.45	-0.10
626	18.44	3.14	23.43	-1.46	0.59	-105.57	-0.29
627	18.46	3.09	23.27	-1.21	0.81	-105.69	-0.07
628	18.48	3.12	23.35	-1.49	0.54	-105.82	-0.34
629	18.50	3.00	22.93	-1.31	0.63	-105.94	-0.25
630	18.52	3.11	23.32	-1.47	0.55	-106.06	-0.33
631	18.54	3.57	24.87	-1.58	0.77	-106.19	-0.11
632	18.56	3.26	23.84	-2.08	0.05	-106.31	-0.83
633	18.58	3.33	24.07	-1.57	0.61	-106.43	-0.27
634	18.60	3.33	24.09	-1.95	0.24	-106.56	-0.65
635	18.62	3.17	23.55	-1.39	0.68	-106.68	-0.20
636	18.64	2.97	22.83	-0.89	1.03	-106.80	0.15
637	18.65	3.09	23.24	-0.87	1.14	-106.93	0.25
638	18.67	3.54	24.76	-1.82	0.50	-107.05	-0.39
639	18.69	3.19	23.60	-1.07	1.01	-107.17	0.12
641	18.73	3.05	23.12	-0.73	1.25	-107.42	0.36
642	18.75	3.00	22.95	-0.66	1.29	-107.54	0.39
643	18.77	2.85	22.38	-0.51	1.32	-107.67	0.42
644	18.79	3.01	22.96	-1.26	0.69	-107.79	-0.21
645	18.81	3.19	23.61	-1.43	0.66	-107.91	-0.24
646	18.83	3.17	23.55	-1.23	0.84	-108.03	-0.05
647	18.85	3.73	25.33	-0.83	1.61	-108.15	0.72
648	18.87	3.48	24.59	-2.25	0.04	-108.27	-0.86
649	18.89	3.06	23.14	-1.57	0.42	-108.39	-0.48
650	18.91	3.31	24.01	-2.07	0.10	-108.51	-0.80
651	18.93	3.60	24.97	-1.65	0.71	-108.61	-0.19
652	18.94	2.85	22.36	-1.22	0.60	-108.70	-0.30
653	18.96	3.21	23.69	-0.99	1.11	-108.80	0.21
654	18.97	3.20	23.66	-1.19	0.90	-108.90	0.00
655	18.99	3.05	23.10	-1.13	0.85	-108.99	-0.06
656	19.01	3.08	23.23	-1.54	0.47	-109.09	-0.44
657	19.02	2.94	22.70	-0.73	1.17	-109.19	0.26
658	19.04	3.16	23.50	-0.94	1.12	-109.29	0.21
659	19.05	3.04	23.09	-0.93	1.05	-109.38	0.14
660	19.07	2.79	22.12	-1.41	0.36	-109.48	-0.54
661	19.09	2.66	21.61	-1.28	0.39	-109.58	-0.52
662	19.10	2.91	22.57	-1.01	0.86	-109.67	-0.05
663	19.12	3.02	22.99	-1.13	0.83	-109.77	-0.09
664	19.13	2.82	22.26	-0.98	0.82	-109.87	-0.09
665	19.15	2.95	22.74	-1.03	0.87	-109.96	-0.04
666	19.16	3.29	23.97	-0.83	1.33	-110.06	0.42
667	19.18	3.36	24.19	-1.29	0.92	-110.16	0.00
668	19.20	3.06	23.15	-1.55	0.44	-110.26	-0.48
669	19.21			-0.88	-3.71	-110.35	-4.63

Depth (cm)	Age (ka) from model	Mg/Ca (mmol/mol)	SST (C°)	$\delta^{18}O$ ‰ (VPDB)	$\delta^{18}O_{sw}$‰ (VSMOW)	Sea Level Change (m)	$\delta^{18}O_{sw\text{-}ivc}$‰ (VSMOW)
670	19.23	3.21	23.66	-0.88	1.22	-110.45	0.30
671	19.24	3.35	24.14	-0.54	1.65	-110.55	0.74
672	19.26	3.30	24.00	-0.54	1.63	-110.64	0.71
673	19.28	3.27	23.89	-0.40	1.74	-110.74	0.82
675	19.31						
676	19.32	3.25	23.83	-1.02	1.11	-111.03	0.19
677	19.34			-1.19	-4.02	-111.13	-4.95
678	19.36	3.47	24.55	-0.66	1.62	-111.23	0.70
679	19.37	3.12	23.36	-0.76	1.27	-111.32	0.35
680	19.39	3.14	23.42	-0.90	1.15	-111.42	0.22
681	19.40	3.05	23.10	-0.96	1.02	-111.52	0.09
682	19.42	2.91	22.60	-1.24	0.64	-111.62	-0.29
683	19.44	3.01	22.96	-1.59	0.36	-111.72	-0.56
684	19.45	3.13	23.38	-1.26	0.78	-111.83	-0.15
685	19.47	3.33	24.09	-1.30	0.88	-111.93	-0.05
686	19.49	3.18	23.58	-1.29	0.78	-112.03	-0.15
687	19.51	3.22	23.71	-1.09	1.02	-112.13	0.09
688	19.52	3.21	23.68	-1.72	0.38	-112.24	-0.55
689	19.54	3.01	22.96	-1.30	0.65	-112.34	-0.29
691	19.57	2.96	22.77	-1.42	0.49	-112.55	-0.44
692	19.59	3.41	24.37	-1.88	0.36	-112.65	-0.57
693	19.61	3.42	24.37	-1.47	0.78	-112.75	-0.16
694	19.62			-0.86	-3.70	-112.86	-4.63
695	19.64			-1.41	-4.24	-112.97	-5.18
696	19.66	3.17	23.53	-1.35	0.72	-113.07	-0.22
697	19.67	3.32	24.07	-0.60	1.58	-113.18	0.64
698	19.69	3.09	23.25	-0.91	1.10	-113.28	0.16
699	19.71	3.00	22.93	-1.10	0.84	-113.39	-0.10
700	19.73	3.33	24.08	-0.80	1.38	-113.50	0.44
701	19.75	3.39	24.30	-0.78	1.45	-113.64	0.51
702	19.77	3.19	23.63	-1.07	1.02	-113.77	0.07
703	19.79	3.05	23.12	-1.26	0.72	-113.91	-0.22
704	19.81	3.25	23.83	-1.23	0.90	-114.04	-0.05
705	19.83	2.94	22.71	-0.65	1.25	-114.17	0.30
706	19.86	3.11	23.32	-0.59	1.43	-114.30	0.48
707	19.88	3.16	23.49	-1.00	1.06	-114.42	0.11
708	19.90	2.91	22.59	-1.14	0.73	-114.55	-0.22
709	19.92	2.88	22.47	-1.25	0.60	-114.68	-0.35
710	19.94	2.75	21.98	-1.36	0.39	-114.80	-0.57
711	19.97	2.96	22.79	-1.45	0.46	-114.93	-0.49
712	19.99	3.00	22.93	-1.20	0.74	-115.06	-0.21
713	20.01	3.03	23.05	-1.41	0.56	-115.18	-0.40
714	20.03	2.98	22.87	-0.79	1.14	-115.31	0.18
715	20.05	2.90	22.55	-1.14	0.72	-115.44	-0.23
716	20.07	3.28	23.92	-0.92	1.23	-115.56	0.27
717	20.10	3.08	23.21	-1.33	0.67	-115.69	-0.29
718	20.12	3.08		-1.08		-115.81	
719	20.14	3.14	23.43	-1.19	0.86	-115.93	-0.10
720	20.16						
721	20.18	3.29	23.96	-0.63	1.53	-116.16	0.56
722	20.21	2.97	22.81	-1.23	0.69	-116.28	-0.28
723	20.23	3.08	23.23	-1.06	0.95	-116.40	-0.02
724	20.25	3.11	23.33	-1.56	0.47	-116.52	-0.50
725	20.27						
726	20.30	3.15	23.49	-1.33		-116.77	
727	20.32	3.14	23.43	-0.75	1.30	-116.90	0.33

Depth (cm)	Age (ka) from model	Mg/Ca (mmol/mol)	SST (C°)	$\delta^{18}O$ ‰ (VPDB)	$\delta^{18}O_{sw}$‰ (VSMOW)	Sea Level Change (m)	$\delta^{18}O_{sw\text{-}ivc}$‰ (VSMOW)
728	20.34	3.02	23.01	-1.73	0.23	-117.04	-0.74
729	20.37			-1.37		-117.17	
730	20.39	3.00	22.95	-1.43	0.52	-117.30	-0.46
731	20.42	2.71	21.78	-1.17	0.53	-117.44	-0.44
732	20.44					-117.57	
733	20.47	2.92	22.61	-1.45	0.43	-117.71	-0.55
734	20.49					-117.84	
735	20.52	3.31	24.03	-1.13	1.04	-117.97	0.06
736	20.54			-1.66		-118.11	
737	20.57	3.03	23.02	-1.49	0.47	-118.24	-0.51
738	20.59	3.26	23.85	-0.85	1.28	-118.37	0.30
739	20.62					-118.51	
740	20.64	3.29	23.94	-1.73	0.42	-118.64	-0.56
741	20.66	3.17	23.53	-0.66	1.41	-118.77	0.42
742	20.69	3.20	23.65	-0.83	1.26	-118.91	0.28
743	20.71	2.91	22.57	-1.35	0.52	-119.04	-0.47
744	20.74	3.11	23.34	-1.14	0.89	-119.17	-0.10
745	20.76	3.05	23.10	0.23	2.21	-119.31	1.22
746	20.79	3.03	23.05				
747	20.81	3.17	23.52	-1.42	0.65	-119.57	-0.35
748	20.84	3.36	24.20				
749	20.86	3.08	23.21	-0.85	1.15	-119.84	0.16
750	20.89						
751	20.91	3.13	23.38	-0.75	1.29	-120.09	0.29
752	20.93	3.20	23.65	-1.12	0.97	-120.21	-0.03
753	20.95	3.33	24.09	-1.04	1.14	-120.32	0.15
754	20.97	2.98	22.86		1.93	-120.43	0.93
755	21.00			-1.35		-120.54	
756	21.02	2.77	22.05			-120.66	
757	21.04	3.31	24.02	-1.12	1.05	-120.77	0.05
758	21.06	3.04	23.07	-1.47	0.50	-120.88	-0.50
759	21.09	3.14	23.43	-1.24	0.81	-121.00	-0.20
761	21.13	2.94	22.69	-1.31	0.58	-121.22	-0.43
762	21.15	3.15	23.48	-3.08	-1.02	-121.34	-2.03
763	21.17	3.01	22.98	-1.04	0.91	-121.45	-0.09
764	21.20	2.69	21.73	-1.90	-0.21	-121.56	-1.22
765	21.22	2.33	20.11	-1.30	0.06	-121.68	-0.95
766	21.24	2.85	22.36	-1.34	0.48	-121.79	-0.53
767	21.26						
768	21.29	3.04	23.07	-1.14	0.84	-122.02	-0.18
769	21.31	3.11	23.33	-1.85	0.18	-122.13	-0.84
770	21.33	3.02	23.02	-1.12	0.84	-122.24	-0.17
771	21.35			-1.05		-122.35	
772	21.37	2.99	22.90	-1.22	0.71	-122.46	-0.30
773	21.40			-1.51		-122.57	
774	21.42			-0.95		-122.68	
775	21.44	2.96	22.78	-1.46	0.45	-122.79	-0.57
776	21.46	3.30	23.99	-0.86	1.30	-122.90	0.28
777	21.48	2.90	22.54	-2.35	-0.49	-123.01	-1.51
778	21.51	3.16	23.52	-0.60	1.47	-123.12	0.44
779	21.53	3.17	23.55	-1.91	0.16	-123.23	-0.86
780	21.55	3.09	23.26	-1.07	0.94	-123.34	-0.08
781	21.57	2.80	22.15	-1.39	0.39	-123.45	-0.64
782	21.59			-1.84		-123.55	
783	21.62	2.98	22.86	-1.51	0.42	-123.66	-0.61
784	21.64			-1.21		-123.77	

Depth (cm)	Age (ka) from model	Mg/Ca (mmol/mol)	SST (C°)	$\delta^{18}O$ ‰ (VPDB)	$\delta^{18}O_{sw}$‰ (VSMOW)	Sea Level Change (m)	$\delta^{18}O_{sw\text{-}ivc}$‰ (VSMOW)
785	21.66			-1.89		-123.88	
786	21.68	2.92	22.62	-2.12	-0.25	-123.99	-1.27
787	21.70			-2.52		-124.10	
788	21.72			-1.29		-124.20	
789	21.75			-1.08		-124.31	
790	21.77			-1.59		-124.42	
791	21.79			-3.06		-124.53	
792	21.81					-124.64	
793	21.83	3.16	23.51	-1.03	1.03	-124.75	-0.01
794	21.85	2.68	21.69	-1.04	0.64	-124.86	-0.40
795	21.88			-1.56		-124.96	
796	21.90					-125.07	
797	21.92			-2.49		-125.18	
798	21.94			-1.93		-125.29	
799	21.96			-0.81		-125.39	
800	21.99	2.89	22.50	-0.61	1.25	-125.50	0.20
801	22.01	3.27	23.90	-0.99	1.16	-125.61	0.12
802	22.03	3.14	23.42	-1.64	0.41	-125.71	-0.64
803	22.05	3.00	22.93	-1.06	0.88	-125.82	-0.16
804	22.07	3.51	24.67	-1.34	0.97	-125.91	-0.08
805	22.09			-1.41		-126.00	
806	22.11			-1.38		-126.08	
807	22.12	3.29	23.94	-2.04	0.12	-126.17	-0.93
808	22.14	3.31	24.04	-1.51	0.66	-126.26	-0.38
809	22.16	3.22	23.71	-1.24	0.86	-126.35	-0.18
810	22.18	3.25	23.81	-1.44	0.69	-126.44	-0.36
811	22.20	3.43	24.41	-1.41	0.84	-126.53	-0.21
812	22.21	3.23	23.76	-1.20	0.91	-126.61	-0.14
813	22.23	3.32	24.04	-0.86	1.31	-126.70	0.26
814	22.25	3.37	24.22	-1.38	0.83	-126.79	-0.22
815	22.27	3.32	24.05	-0.96	1.22	-126.88	0.17
816	22.29	3.18	23.59	-0.74	1.34	-126.97	0.29
817	22.30	2.91	22.58	-2.07	-0.20	-127.05	-1.25
818	22.32	3.09	23.27	-1.76	0.25	-127.14	-0.80
819	22.34	3.02	22.99	-1.07	0.88	-127.23	-0.17
820	22.36	3.13	23.41	-1.31	0.73	-127.32	-0.33
821	22.38	3.26	23.85	-1.85	0.28	-127.41	-0.78
822	22.39	3.01	22.98	-1.57	0.39	-127.49	-0.67
823	22.41	3.34	24.12	-1.10	1.09	-127.58	0.03
824	22.43	3.02	23.00	-1.23	0.73	-127.67	-0.33
825	22.45			-1.23		-127.76	
826	22.46	2.61	21.37	-1.28	0.34	-127.84	-0.72
827	22.48	2.87	22.43	-0.97	0.87	-127.92	-0.20
828	22.50	3.22	23.71	-1.19	0.92	-128.01	-0.15
829	22.52	2.95	22.75	-0.86	1.04	-128.09	-0.02
830	22.53	2.61	21.39	-0.95	0.67	-128.17	-0.39
831	22.55	2.83	22.27	-1.11	0.69	-128.26	-0.37
832	22.57	3.03	23.03	-1.85	0.11	-128.34	-0.95
833	22.58	2.99	22.88	-0.71	1.22	-128.43	0.15
834	22.60	2.92	22.63	-0.75	1.13	-128.51	0.07
835	22.62	3.22	23.70	-1.82	0.28	-128.59	-0.78
836	22.64	3.36	24.18	-1.56	0.64	-128.68	-0.43
837	22.65	3.34	24.12	-1.08	1.11	-128.76	0.04
838	22.67	3.17	23.54	-0.82	1.25	-128.84	0.18
839	22.69	3.49	24.61	-1.35	0.94	-128.93	-0.13
840	22.70	3.16	23.52	-0.84	1.22	-129.01	0.15

Depth (cm)	Age (ka) from model	Mg/Ca (mmol/mol)	SST (C°)	$\delta^{18}O$ ‰ (VPDB)	$\delta^{18}O_{sw}$‰ (VSMOW)	Sea Level Change (m)	$\delta^{18}O_{sw\text{-}ivc}$‰ (VSMOW)
841	22.72	3.79	25.53	-1.08	1.40	-129.09	0.33
842	22.74	3.58	24.90	-1.67	0.69	-129.18	-0.39
843	22.76			-2.19		-129.26	
844	22.77			-3.09		-129.34	
845	22.79	3.40	24.31	-0.34	1.89	-129.43	0.82
846	22.81	3.37	24.22	-0.81	1.40	-129.51	0.32
847	22.82			-0.61		-129.59	
848	22.84			-1.65		-129.68	
849	22.86			-0.94		-129.76	
850	22.87			-1.21		-129.84	
851	22.89			-0.72		-129.93	
852	22.91	3.55	24.80	-1.40	0.93	-130.01	-0.15
853	22.93	3.18	23.56	-1.01	1.06	-130.09	-0.02
854	22.94	2.93	22.66	-0.53	1.36	-130.17	0.28
855	22.96	3.25	23.81	-1.12	1.00	-130.25	-0.08
856	22.98	2.99	22.89	-2.16	-0.22	-130.34	-1.30
857	22.99	3.11	23.34	-2.26	-0.23	-130.42	-1.31
858	23.01	3.04	23.08	-0.61	1.36	-130.50	0.28
859	23.03	2.95	22.74	-0.86	1.04	-130.58	-0.04
860	23.04	3.15	23.46	-1.01	1.04	-130.66	-0.04
861	23.06	3.61	25.00	-0.95	1.43	-130.74	0.34
862	23.08			-1.03		-130.82	
863	23.09			-0.28		-130.91	
864	23.11	3.21	23.68	-0.21	1.89	-130.99	0.81
865	23.13			-1.21		-131.07	
866	23.14			-0.92		-131.15	
867	23.16					-131.23	
868	23.18			-2.30		-131.31	
869	23.19					-131.39	
870	23.21	2.90	22.55			-131.46	
871	23.23	3.00	22.93	-1.32	0.62	-131.54	-0.47
872	23.24	2.88	22.47	-1.08	0.76	-131.62	-0.33
873	23.26	2.68	21.69	-1.68	0.00	-131.70	-1.09
874	23.28			-3.44		-131.78	
875	23.29			-1.33		-131.85	
876	23.31			-3.07		-131.93	
877	23.32					-132.01	
878	23.34	2.74	21.92	-1.35	0.38	-132.08	-0.72
879	23.36			-1.57		-132.16	
880	23.37	2.57	21.23	-1.37	0.22	-132.24	-0.88
881	23.39	2.66	21.61	-1.95	-0.28	-132.32	-1.38
882	23.41	2.39	20.40	-1.33	0.08	-132.39	-1.02
883	23.42	2.81	22.20	-0.33	1.46	-132.47	0.36
884	23.44			-0.92		-132.55	
885	23.45			-1.71		-132.63	
886	23.47	2.85	22.35	-2.28	-0.45	-132.70	-1.56
887	23.49			-3.58		-132.78	
888	23.50	2.47	20.75	-1.68	-0.19	-132.86	-1.29
889	23.52			-2.44		-132.93	
890	23.54					-133.01	
891	23.55			-1.21		-133.09	
892	23.57	2.89	22.51	-1.15	0.70	-133.17	-0.40
893	23.58	3.39	24.29	-1.01	1.22	-133.24	0.11
894	23.60	3.37	24.23	-1.34	0.87	-133.32	-0.23
895	23.62	3.25	23.81	-1.64	0.49	-133.40	-0.62
896	23.63	3.34	24.13	-1.72	0.48	-133.47	-0.63

Depth (cm)	Age (ka) from model	Mg/Ca (mmol/mol)	SST (C°)	$\delta^{18}O$ ‰ (VPDB)	$\delta^{18}O_{sw}$‰ (VSMOW)	Sea Level Change (m)	$\delta^{18}O_{sw\text{-}ivc}$‰ (VSMOW)
897	23.65	3.36	24.18			-133.55	
898	23.66	3.06	23.16	-1.02	0.97	-133.63	-0.14
899	23.68	3.33	24.07	2.41	4.59	-133.71	3.48
900	23.70	3.60	24.97	-1.55	0.81	-133.78	-0.30
901	23.71	3.53	24.73	-1.29	1.03	-133.86	-0.08
902	23.73			-1.13		-133.94	
903	23.75	3.32	24.05	-0.60	1.57	-134.01	0.46
904	23.77	3.36	24.20	-1.35	0.85	-134.14	-0.26
905	23.80	3.31	24.02	-1.31	0.86	-134.27	-0.25
906	23.82	3.25	23.83	-1.03	1.10	-134.39	-0.01
907	23.85			-1.17		-134.52	
908	23.88			-1.50		-134.64	

APPENDIX A (continued)

Data for Core MD02-2550 from 622-908 cm

Table A2. Samples for Core MD02-2550 from 622-908 cm (18.36-23.88 ka): Salinity estimates based on three plausible end-members (EM).

Depth (cm)	Age (ka) from model	$\delta^{18}O_{sw\text{-}ivc}$‰ (VSMOW)	Salinity (EM -7‰)	Salinity (EM-30‰)	Salinity (EM-40‰)
622	18.36	-0.70	28.16	34.42	34.96
623	18.38	-0.66	28.33	34.46	34.99
624	18.40	-0.55	28.85	34.60	35.09
625	18.42	-0.10	30.85	35.12	35.49
626	18.44	-0.29	29.99	34.90	35.32
627	18.46	-0.07	30.98	35.16	35.52
628	18.48	-0.34	29.78	34.84	35.28
629	18.50	-0.25	30.19	34.95	35.36
630	18.52	-0.33	29.83	34.86	35.29
631	18.54	-0.11	30.78	35.11	35.48
632	18.56	-0.83	27.59	34.27	34.84
633	18.58	-0.27	30.08	34.92	35.34
634	18.60	-0.65	28.39	34.48	35.00
635	18.62	-0.20	30.38	35.00	35.40
636	18.64	0.15	31.94	35.41	35.71
637	18.65	0.25	32.41	35.53	35.80
638	18.67	-0.39	29.57	34.79	35.24
639	18.69	0.12	31.84	35.39	35.69
641	18.73	0.36	32.91	35.66	35.90
642	18.75	0.39	33.05	35.70	35.93
643	18.77	0.42	33.19	35.74	35.96
644	18.79	-0.21	30.37	35.00	35.40
645	18.81	-0.24	30.22	34.96	35.37
646	18.83	-0.05	31.05	35.18	35.53
647	18.85	0.72			
648	18.87	-0.86	27.45	34.23	34.82
649	18.89	-0.48	29.14	34.67	35.15
650	18.91	-0.80	27.70	34.30	34.87
651	18.93	-0.19	30.45	35.02	35.41
652	18.94	-0.30	29.96	34.89	35.32
653	18.96	0.21	32.22	35.48	35.77
654	18.97	0.00	31.29	35.24	35.58
655	18.99	-0.06	31.04	35.17	35.53
656	19.01	-0.44	29.33	34.72	35.19
657	19.02	0.26	32.45	35.54	35.81
658	19.04	0.21	32.25	35.49	35.77
659	19.05	0.14	31.91	35.40	35.70
660	19.07	-0.54	28.86	34.60	35.10
661	19.09	-0.52	28.97	34.63	35.12
662	19.10	-0.05	31.06	35.18	35.54
663	19.12	-0.09	30.91	35.14	35.50
664	19.13	-0.09	30.89	35.14	35.50
665	19.15	-0.04	31.11	35.19	35.55
666	19.16	0.42	33.15	35.73	35.95
667	19.18	0.00	31.30	35.24	35.58
668	19.20	-0.48	29.16	34.68	35.16

Depth (cm)	Age (ka) from model	$\delta^{18}O_{sw\text{-}ivc}$‰ (VSMOW)	Salinity (EM -7‰)	Salinity (EM-30‰)	Salinity (EM-40‰)
669	19.21	-4.63			
670	19.23	0.30	32.63	35.59	35.85
671	19.24	0.74			
672	19.26	0.71	34.45	36.07	36.21
673	19.28	0.82	34.97	36.21	36.31
675	19.31				
676	19.32	0.19	32.14	35.46	35.75
677	19.34	-4.95			
678	19.36	0.70	34.41	36.06	36.20
679	19.37	0.35	32.85	35.65	35.89
680	19.39	0.22	32.28	35.50	35.78
681	19.40	0.09	31.70	35.35	35.66
682	19.42	-0.29	30.00	34.90	35.32
683	19.44	-0.56	28.77	34.58	35.08
684	19.45	-0.15	30.62	35.06	35.45
685	19.47	-0.05	31.07	35.18	35.54
686	19.49	-0.15	30.64	35.07	35.45
687	19.51	0.09	31.67	35.34	35.66
688	19.52	-0.55	28.82	34.59	35.09
689	19.54	-0.29	30.01	34.90	35.33
691	19.57	-0.44	29.31	34.72	35.19
692	19.59	-0.57	28.73	34.57	35.07
693	19.61	-0.16	30.58	35.05	35.44
694	19.62	-4.63			
695	19.64	-5.18			
696	19.66	-0.22	30.32	34.98	35.39
697	19.67	0.64	34.15	35.99	36.15
698	19.69	0.16	32.01	35.43	35.72
699	19.71	-0.10	30.85	35.12	35.49
700	19.73	0.44	33.26	35.76	35.97
701	19.75	0.51	33.55	35.83	36.03
702	19.77	0.07	31.62	35.33	35.65
703	19.79	-0.22	30.30	34.98	35.38
704	19.81	-0.05	31.09	35.19	35.54
705	19.83	0.30	32.63	35.59	35.85
706	19.86	0.48	33.46	35.81	36.01
707	19.88	0.11	31.78	35.37	35.68
708	19.90	-0.22	30.31	34.98	35.39
709	19.92	-0.35	29.71	34.82	35.27
710	19.94	-0.57	28.75	34.57	35.08
711	19.97	-0.49	29.10	34.66	35.14
712	19.99	-0.21	30.34	34.99	35.39
713	20.01	-0.40	29.51	34.77	35.23
714	20.03	0.18	32.11	35.46	35.74
715	20.05	-0.23	30.25	34.97	35.37
716	20.07	0.27	32.50	35.56	35.82
717	20.10	-0.29	30.00	34.90	35.32
718	20.12		31.11	35.19	35.54
719	20.14	-0.10	30.83	35.12	35.49
720	20.16				
721	20.18	0.56	33.81	35.90	36.08
722	20.21	-0.28	30.05	34.91	35.33
723	20.23	-0.02	31.20	35.22	35.56
724	20.25	-0.50	29.05	34.65	35.14
725	20.27				
726	20.30		30.22	34.96	35.37

Depth (cm)	Age (ka) from model	$\delta^{18}O_{sw\text{-}ivc}$‰ (VSMOW)	Salinity (EM -7‰)	Salinity (EM-30‰)	Salinity (EM-40‰)
727	20.32	0.33	32.75	35.62	35.87
728	20.34	-0.74	27.98	34.37	34.92
729	20.37				
730	20.39	-0.46	29.25	34.70	35.17
731	20.42	-0.44	29.31	34.72	35.19
732	20.44				
733	20.47	-0.55	28.85	34.60	35.10
734	20.49				
735	20.52	0.06	31.58	35.31	35.64
736	20.54				
737	20.57	-0.51	29.01	34.64	35.13
738	20.59	0.30	32.64	35.59	35.85
739	20.62				
740	20.64	-0.56	28.79	34.58	35.08
741	20.66	0.42	33.18	35.74	35.96
742	20.69	0.28	32.53	35.56	35.83
743	20.71	-0.47	29.19	34.69	35.16
744	20.74	-0.10	30.85	35.12	35.49
745	20.76	1.22	36.74		36.67
746	20.79				
747	20.81	-0.35	29.75	34.83	35.27
748	20.84				
749	20.86	0.16	31.99	35.42	35.72
750	20.89				
751	20.91	0.29	32.59	35.58	35.84
752	20.93	-0.03	31.16	35.21	35.55
753	20.95	0.15	31.95	35.41	35.71
754	20.97	0.93			36.41
755	21.00				
756	21.02				
757	21.04	0.05	31.51	35.30	35.62
758	21.06	-0.50	29.04	34.65	35.13
759	21.09	-0.20	30.41	35.01	35.41
761	21.13	-0.43	29.38	34.74	35.20
762	21.15	-2.03	22.22	32.86	33.78
763	21.17	-0.09	30.87	35.13	35.50
764	21.20	-1.22	25.83	33.81	34.50
765	21.22	-0.95	27.03	34.12	34.73
766	21.24	-0.53	28.93	34.62	35.11
767	21.26				
768	21.29	-0.18	30.50	35.03	35.42
769	21.31	-0.84	27.55	34.26	34.84
770	21.33	-0.17	30.52	35.04	35.43
771	21.35				
772	21.37	-0.30	29.94	34.89	35.31
773	21.40				
774	21.42				
775	21.44	-0.57	28.75	34.57	35.08
776	21.46	0.28	32.56	35.57	35.83
777	21.48	-1.51	24.53	33.46	34.23
778	21.51	0.44	33.27	35.76	35.98
779	21.53	-0.86	27.44	34.23	34.82
780	21.55	-0.08	30.92	35.14	35.51
781	21.57	-0.64	28.44	34.49	35.01
782	21.59				
783	21.62	-0.61	28.57	34.53	35.04

Depth (cm)	Age (ka) from model	$\delta^{18}O_{sw\text{-}ivc}$‰ (VSMOW)	Salinity (EM -7‰)	Salinity (EM-30‰)	Salinity (EM-40‰)
784	21.64				
785	21.66				
786	21.68	-1.27	25.59	33.74	34.45
787	21.70				
788	21.72				
789	21.75				
790	21.77				
791	21.79				
792	21.81				
793	21.83	-0.01	31.26	35.23	35.58
794	21.85	-0.40	29.52	34.78	35.23
795	21.88				
796	21.90				
797	21.92				
798	21.94				
799	21.96				
800	21.99	0.20	32.21	35.48	35.76
801	22.01	0.12	31.81	35.38	35.68
802	22.03	-0.64	28.45	34.49	35.02
803	22.05	-0.16	30.57	35.05	35.44
804	22.07	-0.08	30.95	35.15	35.51
805	22.09				
806	22.11				
807	22.12	-0.93	27.13	34.15	34.75
808	22.14	-0.38	29.58	34.79	35.24
809	22.16	-0.18	30.47	35.02	35.42
810	22.18	-0.36	29.66	34.81	35.26
811	22.20	-0.21	30.37	35.00	35.40
812	22.21	-0.14	30.68	35.08	35.46
813	22.23	0.26	32.44	35.54	35.81
814	22.25	-0.22	30.31	34.98	35.39
815	22.27	0.17	32.03	35.43	35.73
816	22.29	0.29	32.59	35.58	35.84
817	22.30	-1.25	25.70	33.77	34.47
818	22.32	-0.80	27.71	34.30	34.87
819	22.34	-0.17	30.51	35.04	35.43
820	22.36	-0.33	29.83	34.86	35.29
821	22.38	-0.78	27.83	34.33	34.89
822	22.39	-0.67	28.29	34.45	34.98
823	22.41	0.03	31.45	35.28	35.61
824	22.43	-0.33	29.81	34.85	35.29
825	22.45				
826	22.46	-0.72	28.07	34.39	34.94
827	22.48	-0.20	30.41	35.01	35.41
828	22.50	-0.15	30.64	35.07	35.45
829	22.52	-0.02	31.20	35.22	35.56
830	22.53	-0.39	29.54	34.78	35.23
831	22.55	-0.37	29.63	34.80	35.25
832	22.57	-0.95	27.03	34.12	34.73
833	22.58	0.15	31.98	35.42	35.72
834	22.60	0.07	31.59	35.32	35.64
835	22.62	-0.78	27.79	34.32	34.88
836	22.64	-0.43	29.38	34.74	35.20
837	22.65	0.04	31.47	35.29	35.62
838	22.67	0.18	32.10	35.45	35.74
839	22.69	-0.13	30.71	35.09	35.46

Depth (cm)	Age (ka) from model	$\delta^{18}O_{sw\text{-}ivc}$‰ (VSMOW)	Salinity (EM -7‰)	Salinity (EM-30‰)	Salinity (EM-40‰)
840	22.70	0.15	31.97	35.42	35.72
841	22.72	0.33	32.76	35.63	35.87
842	22.74	-0.39	29.57	34.79	35.24
843	22.76				
844	22.77				
845	22.79	0.82			
846	22.81	0.32	32.74	35.62	35.87
847	22.82				
848	22.84				
849	22.86				
850	22.87				
851	22.89				
852	22.91	-0.15	30.64	35.07	35.45
853	22.93	-0.02	31.21	35.22	35.56
854	22.94	0.28	32.53	35.57	35.83
855	22.96	-0.08	30.94	35.15	35.51
856	22.98	-1.30	25.47	33.71	34.42
857	22.99	-1.31	25.42	33.70	34.41
858	23.01	0.28	32.53	35.57	35.83
859	23.03	-0.04	31.11	35.19	35.54
860	23.04	-0.04	31.11	35.19	35.54
861	23.06	0.34	32.82	35.64	35.89
862	23.08				
863	23.09				
864	23.11	0.81	34.89		
865	23.13				
866	23.14				
867	23.16				
868	23.18				
869	23.19				
870	23.21				
871	23.23	-0.47	29.19	34.69	35.16
872	23.24	-0.33	29.82	34.85	35.29
873	23.26	-1.09	26.43	33.96	34.61
874	23.28				
875	23.29				
876	23.31				
877	23.32				
878	23.34	-0.72	28.09	34.40	34.94
879	23.36				
880	23.37	-0.88	27.38	34.21	34.80
881	23.39	-1.38	25.13	33.62	34.36
882	23.41	-1.02	26.75	34.05	34.68
883	23.42	0.36	32.90	35.66	35.90
884	23.44				
885	23.45				
886	23.47	-1.56	24.34	33.41	34.20
887	23.49				
888	23.50	-1.29	25.51	33.72	34.43
889	23.52				
890	23.54				
891	23.55				
892	23.57	-0.40	29.49	34.77	35.22
893	23.58	0.11	31.79	35.37	35.68
894	23.60	-0.23	30.25	34.97	35.37
895	23.62	-0.62	28.52	34.51	35.03

Depth (cm)	Age (ka) from model	$\delta^{18}O_{sw\text{-}ivc}$‰ (VSMOW)	Salinity (EM -7‰)	Salinity (EM-30‰)	Salinity (EM-40‰)
896	23.63	-0.63	28.47	34.50	35.02
897	23.65				
898	23.66	-0.14	30.68	35.08	35.46
899	23.68	3.48			
900	23.70	-0.30	29.97	34.89	35.32
901	23.71	-0.08	30.92	35.14	35.51
902	23.73				
903	23.75	0.46	33.34	35.78	35.99
904	23.77	-0.26	30.13	34.93	35.35
905	23.80	-0.25	30.16	34.94	35.36
906	23.82	-0.01	31.24	35.23	35.57
907	23.85				
908	23.88				
			Slope=0.22	Slope=0.85	Slope=1.12